JACC: BASIC TO TRANSLATIONAL SCIENCE VOL. 9, NO. 4, 2024

ORIGINAL RESEARCH - PRECLINICAL

Mitochondrial Ca^{2+} Uniporter–Dependent Energetic Dysfunction Drives Hypertrophy in Heart Failure

Hugo Alves-Figueiredo, PhD,[a,b,c] Christian Silva-Platas, PhD,[a] Manuel Estrada, PhD,[d] Yuriana Oropeza-Almazán, PhD,[a] Martin Ramos-González, MD, PhD,[a] Judith Bernal-Ramírez, PhD,[a,b] Eduardo Vázquez-Garza, MD, PhD,[a,b] Armando Tellez, PhD,[a,e] Felipe Salazar-Ramírez, MD, MSc,[a] Abraham Méndez-Fernández, MSc,[a] José Luis Galaz, MD,[d] Pedro Lobos, PhD,[d] Keith Youker, PhD,[f] Omar Lozano, PhD,[a,b,c] Guillermo Torre-Amione, MD, PhD,[a,c,f] Gerardo García-Rivas, PhD[a,b,c]

VISUAL ABSTRACT

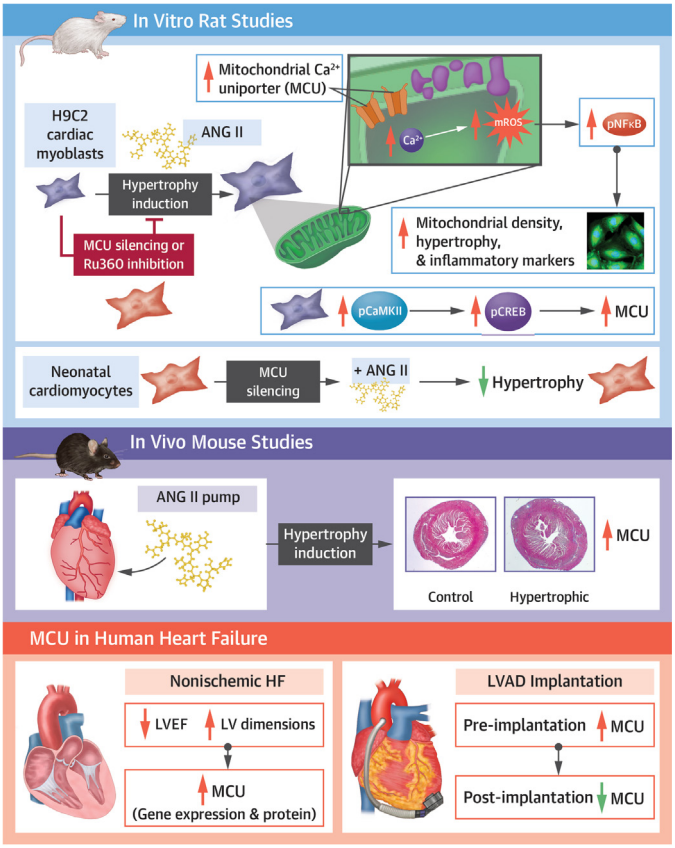

Alves-Figueiredo H, et al. J Am Coll Cardiol Basic Trans Science. 2024;9(4):496-518.

HIGHLIGHTS

- **The MCU is upregulated in ANGII-induced hypertrophic cardiomyocytes inducing mitochondrial calcium overload, energetic dysfunction, and mitochondrial ROS-dependent activation of NFKB.**
- **ANG II induced MCU upregulation through activation of calcium-dependent CREB/CaMKII signaling.**
- **Targeting the MCU, whether by gene silencing or pharmacological inhibition, results in the successful prevention of cellular hypertrophy and energetic dysfunction induced by ANG II.**
- **MCU is upregulated in mouse hypertrophic hearts and in remodeled human left ventricles suffering from nonischemic heart failure.**
- **MCU expression is reduced in the left ventricles of patients following the implantation of a Left Ventricular Assist Device.**

ISSN 2452-302X https://doi.org/10.1016/j.jacbts.2024.01.007

SUMMARY

The role of the mitochondrial calcium uniporter (MCU) in energy dysfunction and hypertrophy in heart failure (HF) remains unknown. In angiotensin II (ANGII)-induced hypertrophic cardiac cells we have shown that hypertrophic cells overexpress MCU and present bioenergetic dysfunction. However, by silencing MCU, cell hypertrophy and mitochondrial dysfunction are prevented by blocking mitochondrial calcium overload, increase mitochondrial reactive oxygen species, and activation of nuclear factor kappa B-dependent hypertrophic and proinflammatory signaling. Moreover, we identified a calcium/calmodulin-independent protein kinase II/cyclic adenosine monophosphate response element-binding protein signaling modulating MCU upregulation by ANGII. Additionally, we found upregulation of MCU in ANGII-induced left ventricular HF in mice, and in the LV of HF patients, which was correlated with pathological remodeling. Following left ventricular assist device implantation, MCU expression decreased, suggesting tissue plasticity to modulate MCU expression.
(J Am Coll Cardiol Basic Trans Science 2024;9:496–518)

ABBREVIATIONS AND ACRONYMS

$\Delta\Psi$ = mitochondrial membrane potential

ATP = adenosine triphosphate

Ca^{2+} = calcium

CAMKII = calcium/calmodulin-dependent protein kinase II

CM = cardiomyopathy

CRC = calcium retention capacity

CREB = cyclic adenosine monophosphate response element-binding protein

HF = heart failure

LV = left ventricle

LVAD = left ventricle assist device implantation

MCU = mitochondrial calcium uniporter

mPTP = mitochondrial permeability transition pore

mROS = mitochondrial reactive oxygen species

NADH = nicotinamide adenine dinucleotide hydrogen

Ru_{360} = ruthenium 360

Cardiac function is driven by calcium (Ca^{2+}) cycling and excitation-contraction coupling, which requires a dynamic energy supply system.[1] Ca^{2+} has been recognized as a second messenger that coordinates changes in cytosolic workload with mitochondrial energy metabolism in cardiomyocytes. Under physiological conditions, mitochondrial Ca^{2+} (mCa^{2+}) handling serves as a signal to regulate mitochondrial energy output and link cardiac energy supply to contractile demand.[2,3] However, in the failing heart, mCa^{2+} mishandling is one of the major contributors responsible for mitochondrial dysfunction, impaired bioenergetics, and cell survival.[4,5] The major pathway for mCa^{2+} uptake is through the mitochondrial Ca^{2+} uniporter (MCU) complex. Recent developments in its identification have increased speculation about its role in the pathophysiology of heart failure (HF). This transmembrane protein is composed of 2 transmembrane domains that have a selective Ca^{2+} affinity that facilitates the voltage-dependent transport of Ca^{2+} across the mitochondrial inner membrane.[6]

The MCU complex is composed at the inner mitochondrial membrane by the MCU pore and by regulatory subunits essential MCU regulator (EMRE) and mitochondrial calcium uniporter dominant negative beta subunit (MCUb), and in the intermembrane space are regulators mitochondrial calcium uptake 1, 2 and 3 (MICU1, MICU2, and MICU3), which are known to regulate Ca^{2+} gating/tolerance.[7] Upon stimulation, the sarcoplasmic reticulum releases Ca^{2+}, which is sensed by the MCU complex in proximity, and, depending on its cooperativity, may activate Ca^{2+} uptake into the mitochondria.[8,9] The rise in mCa^{2+} activates Ca^{2+}-dependent dehydrogenases from the Krebs cycle, increasing the capacity to produce nicotinamide adenine dinucleotide hydrogen (NADH).[8,9] The respiratory chain then oxidizes NADH, increasing myocardial volume oxygen (MVO_2) consumption to establish the proton gradient to produce adenosine triphosphate (ATP) by oxidative phosphorylation.[8,9] ATP is removed from the mitochondria through a creatine kinase system.[8,9]

Pharmacologic inhibition of the MCU with ruthenium 360 (Ru_{360}), a specific MCU inhibitor that targets aspartate residues in the DXXE motif in the

From the [a]Tecnologico de Monterrey, Escuela de Medicina y Ciencias de la Salud, Cátedra de Cardiología y Medicina Vascular, Monterrey, NL, México; [b]Tecnologico de Monterrey, Institute for Obesity Research, Monterrey, NL, México; [c]Tecnologico de Monterrey, Hospital Zambrano Hellion, TecSalud, San Pedro Garza García, NL, México; [d]Programa de Fisiología y Biofísica, Facultad de Medicina, Instituto de Ciencias Biomédicas (ICBM), Universidad de Chile, Santiago, Chile; [e]Alizée Pathology, Thurmont, Maryland, USA; and the [f]Weill Cornell Medical College, Methodist DeBakey Heart & Vascular Center, The Methodist Hospital, Houston, Texas, USA.

The authors attest they are in compliance with human studies committees and animal welfare regulations of the authors' institutions and Food and Drug Administration guidelines, including patient consent where appropriate. For more information, visit the Author Center.

Manuscript received October 12, 2023; revised manuscript received January 5, 2024, accepted January 8, 2024.

JACC: BASIC TO TRANSLATIONAL SCIENCE VOL. 9, NO. 4, 2024
APRIL 2024:496–518

pore and decreases β-adrenoceptor response, uncoupling the production of energetic metabolites with workload. This provides the first evidence that workload and energy supply coupling are dependent on mCa^{2+} influx.[10,11] Later studies using animal models of heart-specific deletion of MCU have since corroborated the importance of mCa^{2+} handling in modulating Ca^{2+}-dependent metabolism during stress as well as demonstrated the potential role of MCU in protecting against myocardial injury and cell fate.[8,12]

Nevertheless, there has been no clarity on the role of the mCa^{2+} dynamics in cardiomyocyte plasticity in response to acute and chronic increases in workload. Recent evidence points to an increase in the transcript and protein levels of MCU in response to maladaptive cardiac hypertrophy generated by the chronic increase of workload following transaortic constriction surgery, suggesting this as a potential mechanism for the progression of HF.[13]

In this study, we hypothesized and demonstrated that, in the failing human heart, increased energy demand triggers mCa^{2+} overload through upregulation of the MCU, promoting energetic dysfunction. For the first time, we showed that this mechanism is a determinant in the onset of pathologic hypertrophy.

METHODS

PATIENT RECRUITMENT AND LEFT VENTRICULAR TISSUE COLLECTION. Myocardial tissue samples collected during cardiac transplantation, or left ventricle assist device (LVAD) implantation, and which did not have a primary diagnosis of myocarditis as defined by the Dallas criteria, postpartum cardiomyopathy (CM), congenital CM, hypertrophic CM, and Adriamycin-induced CM were collected from 2000 to 2010 at the Methodist Hospital, Houston Texas. Tissue samples were obtained from the left ventricular (LV) apex or LV-free wall without adipose tissue and avoiding scar tissue. The investigation conforms with the principles outlined in the Declaration of Helsinki.[14] All samples were collected under an institutional review board-approved protocol (IRB (3N) 0511-0100). A waiver of consent was obtained due to the collection of normally discarded tissues coded at the time of collection with no identifying information.

ANGIOTENSIN II–INDUCED HF MOUSE MODEL. All animal experiments were reviewed and approved by the Institutional Animal Care and Use Committee in accordance with the official Mexican Legislation NOM-062-ZOO-1999. HF was induced in male C57BL/6 mice purchased from Bioinvert. After 1 week of ad libitum administration of 1% sodium chloride (NaCl) and 0.01% of N-nitro L-arginine methyl ester in the drinking water, a micro-osmotic pump was surgically implanted in the subdermal dorsal area diffusing angiotensin II (ANGII) at a rate of 0.7 mg/kg/d.[15] The control group received the same manipulation without the implantation of the pump. Animals were maintained at 25 °C with a 12-hour light/dark cycle. Water and food were given ad libitum.

Euthanasia and tissue collection were performed after 28 days. Euthanasia was performed by cardiotomy under anesthesia with sevoflurane 4%, 500 mL/min O_2. The heart was weighed and LV was dissected and apex subsection was dissected from LV tissue and frozen immediately in liquid nitrogen for further polymerase chain reaction (PCR) analysis or protein expression analysis through Western blot. The remaining LV tissue was collected in a Histosette and placed in paraformaldehyde (PFA) for histopathologic analysis. LV hemodynamics were assessed in vivo through pressure-volume (PV) analysis performed as previously described[16] using an open-heart configuration and a 1.2-Fr PV catheter with the ADV500 PV measurement system (Transonic Scisense).

LV MICROGRAFT ANALYSIS OF FIBROSIS AND HYPERTROPHY. The tissue remained in PFA 4% (wt/vol) in phosphate-buffered saline (PBS) for 24 hours at room temperature. The tissue was processed into a paraffin-embedded block and 3-μm slices were stained. Micrografts were acquired using a bright field microscope (Imager Z.1 Zeiss microscope, with AxioCa HRm). Images were analyzed with AxioVision software.

Fibrosis was assessed using Masson's Trichrome staining, and images were acquired of whole tissue at 1.25 times and 5 times original magnification. Heart hypertrophy was assessed by normalizing heart weight to tibia length, and by analyzing hematoxylin and eosin (HE) staining in sliced tissues. Only cells with a nucleus at the center were considered. At least 20 cells per image were selected. The diameter was measured using Image J software (v1.53t, NIH).

CARDIOMYOCYTE ISOLATION AND CULTURE. All animal-use procedures were in accordance with guidelines approved by the Bioethical Committee at the Facultad de Medicina, Universidad de Chile. Primary neonatal rat cardiomyocytes were purified from hearts of 3-day-old Sprague-Dawley rats, following the protocol previously reported.[17] Purity of the primary culture was at least 95%. The cardiomyocytes

were cultured in Dulbecco's Modified Eagle's Medium (DMEM):M-199 (4:1) supplemented with 10% fetal bovine serum (FBS) and 1% penicillin-streptomycin and 10 μM bromodeoxyuridine to prevent overgrowth of fibroblasts and smooth muscle cells.

CARDIOMYOCYTE TRANSFECTION. Small interference RNA (siRNA) to MCU (siMCU) was designed as previously described.[18] They designed siRNA-MCU calcium 1, sense strand sequence: 5′-CGGCUUACCUGGUGGGAAU-3′. The nontargeting scramble siRNA sequence is the MISSION siRNA Universal Negative Control #1 (SIC001). After 24 hours of culture, cells grown on 60-mm dishes were transfected with siMCU (50 nM) using Lipofectamine 2000 (Invitrogen) according to the manufacturer's instructions and previous reports from our lab.[18]

CARDIOMYOCYTE HYPERTROPHY ASSESSMENT: SARCOMERIZATION AND CELL AREA MEASUREMENT. To evaluate hypertrophy in cardiomyocytes exposed to ANGII, indirect immunofluorescence against the sarcomeric protein α-actinin was performed as described previously to evaluate the complexity grade of sarcomerization produced by hypertrophy.[19] Briefly, confocal z-stacks were acquired and analyzed from the wider range of not-branched myotubes. To quantify cell area, cardiomyocytes were incubated with the vital fluorescent dye cell tracker green (Molecular Probes) for 45 minutes and fluorescent images were acquired (LSM Pascal 5, Zeiss) and analyzed as described previously.[20]

H9C2 CELL CULTURE. H9C2 cells (ATCC) passage 4 were seeded and expanded in T75 cm2 culture flasks in DMEM-high glucose medium (Sigma Aldrish-Merck KGaA), supplemented with 10% of FBS (Biowest Nuaillé), and Penicillin/Streptomycin (100 U/mL penicillin, 100 pg/mL streptomycin) (GE Healthcare Life Sciences, PGH). The cells were cultured at 37 °C under a 5% CO_2 and 95% air-humidified atmosphere. For expansion, cells were passed when they reached a confluency of 80%. Briefly, cells were harvested using trypsin-EDTA 0.25% (BioWest) at 37 °C, washed with PBS, and centrifuged at 1,300 rpm/5 min/room temperature (RT). Cells were resuspended in culture media, and after calculating cell concentration using trypan-blue staining and hemocytometer, cells were seeded at the desired amount.

H9C2 CELLS TRANSFECTION. Between approximately 5×10^4 and 10×10^4 H9C2 cells were seeded in 24- or 12-well culture plates, respectively, and transfected using a short hairpin RNA (shRNA) plasmid (GeneCopoeia) with the target sequence designed for MCU (GCCAGAGACAGACAATACT) inserted in a plasmid, with flanked restriction sites for BamH1 and EcoR1, and under a U6 promoter. The construct also contained an enhanced green fluorescent protein (EGFP) coding sequence under a cytomegalovirus promoter to function as a transfection fluorescent reporter and a PuroRcoding sequence to confer puromycin resistance to cells, allowing purification by an imposed selection of the transfected culture. The transfection was performed for 72 hours using 1 to 2.5 ug of coding (shMCU) or non-coding (shMock) DNA, Lipofectamine 3000 and Opti-ME (ThermoFisher), according to the manufacturer's instructions. Finally, cell transfection efficiency and culture purification were assessed as cell EGFP fluorescent cell by total cell (nuclei staining using DRA staining), using confocal microscopy. For EGFP, excitation was induced using a 488-nm laser, and the emission was detected at 517 nm with a bandwidth of 10 nm. For Draq, the 633-nm laser was used for excitation, and emission was detected at 683 nm, with a bandwidth of 33 nm.

IN VITRO INDUCTION OF CELL HYPERTROPHY AND CELL CULTURE TREATMENTS. ANGII was used to induce cell hypertrophy in H9C2 cells. Twenty-four hours following cell seeding, cells were starved off by reducing the amount of FBS supplemented to 1%; this concentration was maintained for the rest of the experiment. Twenty-four hours after starving, 1 μM ANGII (TOCRIS, R&D) was supplemented to medium every 24 hours for 2 days. Additionally, to explore the underlying mechanisms, cells were exposed to specific MCU inhibitor Ru_{360} 1 μM, 48 hours; mitochondrial Na^+/Ca^{2+} exchanger (NCLX) inhibitor, CGP37157, 5 μM, 48 hours; mitochondrial reactive oxygen species (mROS) antioxidant, specific scavenger of mitochondrial superoxide, MitoTEMPO, 10 μM, 48 hours; Ca^{2+} chelator, BAPTA-AM, 5 μM, 24 hours; Ca^{2+}/calmodulin kinase II (CAMKII) inhibitor, KN93, 5 μM, 48 hours; and cyclic adenosine monophosphate response element-binding protein (CREB) inhibitor, 66615 1 μM, 48 hours.

LIVE CELL HYPERTROPHY IMAGING. Cell hypertrophy was assessed by fluorescence using confocal microscopy. Briefly, live cells were seeded in coverslips and loaded with 1 μM calcein-AM (Invitrogen, C34852) for 30 minutes at 37 °C in Tyrode solution and 10 μM of nuclei-staining probe Draq (Thermo Scientific, 62251) immediately before acquiring fluorescent images. Afterwards, coverslips were mounted in a perfusion chamber. Fluorescent XY images were

acquired using a Leica TCS SP5 confocal microscope equipped with a D-apochromatic 40X, 1.2 NA, oil objective (Leica Microsystems). Calcein excitation was induced using a 488-nm laser, and the emission was detected at 517 nm with a bandwidth of 10 nm. For Draq, the 633-nm laser was used to induce excitation and emission was detected at 683 nm with a bandwidth of 33 nm. The area of positive Calcein fluorescence was determined for each cell as a surrogate of cell area. Area quantification was assessed using ImageJ software (NIH).

MCU IMMUNOHISTOCHEMISTRY. Human LV tissue samples were fixed in 4% (wt/vol) PFA in PBS for at least 24 hours at RT, desiccated, embedded in paraffin, and sliced. Following rehydration and microwave antigen retrieval, tissue slices were incubated with MCU antibodies (14997S, CST) at 4 °C overnight and incubated with secondary antibodies at 37 °C for 30 minutes. Bright field microphotographs were acquired using an Imager Z.1 Zeiss microscope with an AxioCam HRm and processed with the AxioVision software.

MCU IMMUNOFLUORESCENCE. To assess the immunofluorescent staining of MCU in transfected shMCU and shMock H9C2 cells, briefly, cells seeded in a multiwell coverglass (Nun Lab-Te, ThermoFisher) were fixed for 20 minutes at 4 °C using PFA 4%. After washing with PBS, cells were permeabilized with a 0.1% Triton X-100-PBS solution for 15 minutes at RT. Then, the cells were once more washed in PBS and then incubated in 0.01% Triton X-100-3% bovine serum albumin (BSA)-PBS blocking solution for 20 minutes at RT. Following this, the cells were incubated with a 1:200 dilution of the primary rabbit antibody against MCU (Cell Signaling) in 0.01% Triton X-100-3% BSA-PBS solution overnight at 4 °C on a rotating table. They were then washed with PBS (4 × 30 minutes) and then incubated with a 1:200 dilution of Alexa Fluo 532 goat anti-rabbit immunoglobulin G (ThermoFisher) for 18 hours at 4 °C, on a rotating table. Finally, cells were mounted with VectaShield mounting medium (Vector Laboratories). Fluorescent images of positive EGFP cells and MCU fluorescence were acquired using confocal microscopy as described previously (see the previous section on Live Cell Hypertrophy Imaging). For MCU-Alexa Fluo 555, excitation was induced using a 535-nm laser and emission was detected at 554 nm with a bandwidth of 20 nm.

mCA^{2+} TRANSPORT RATE AND CA^{2+} RETENTION CAPACITY. Ca^{2+} retention capacity (CRC) is a functional test to quantitatively assess the sensitivity for the mitochondrial permeability transition pore (mPTP) opening due to Ca^{2+} overload. The CRC protocol used by Chapoy-Villanueva et al[21] was implemented in permeabilized cells. In a 48-well plate, 1×10^6 cells were resuspended in 500 mL of respiration buffer with 40 μM ethylene glycol-bis(2-aminoethylether)-N,N,N′,N′-tetraacetic acid (EGTA) containing 40 μM digitonin, 2 μg/mL Rotenone, and 0.3 μM Ca^{2+} green-5N (CG-5N), a Ca^{2+} reporter. CG-5N fluorescence (λex485 nm/λem528 nm) was registered at 25 °C at baseline conditions for 5 minutes. After 5 minutes of signal stabilization, to measure mCa^{2+} transport, 1 bolus of 40 μM Ca^{2+} was added to determine mCa^{2+} transport, followed by the addition of 12.5 mM succinate after signal stabilization to promote mitochondrial Ca^{2+} influx. For CRC, 10 μM Ca^{2+} bolus every 6 minutes was used until mPTP opening. Fluorescence was recorded at 488 nm excitation and 528 nm emission. CRC was determined as the amount of Ca^{2+} boluses buffered by the mitochondria until the opening of the mPTP. In contrast, the Ca^{2+} influx rate was assessed using the same protocol but adding 1 μM Cyclosporin A (CSA) in the respiration media. Influx rate was determined using the derivative of a second-order polynomial regression adjusted to the fluorescence signal decay.

REACTIVE OXYGEN SPECIES QUANTIFICATION BY FLOW CYTOMETRY. mROS content was assessed by flow cytometry using MitoSox (ThermoFisher) as the mitochondrial superoxide indicator. Cells were resuspended in 500 μL of Tyrode with 5 μM MitoSOX, incubated for 10 minutes at 37 °C, and analyzed by flow cytometry measuring fluorescence. At least 20,000 events per sample were analyzed in a FACSCanto II cytometer (BD Biosciences), and triplicates were performed for each set. We performed doublet exclusion for each analysis and analyzed the median fluorescence intensity (MFI) expression of the whole population of MitoSOX (Phycoerythrin [PE] channel) and dichlorofluorescin diacetate (DCFDA) (Fluorescein isothiocyanate [FITC] channel). Data were analyzed using FlowJo V10.

mCa^{2+} CONTENT. To assess mCa^{2+} content, 2×10^6 cells were detached with 2 mL trypsin, washed in 15-mL tubes with 10 mL DMEM+1% FBS to inactivate the trypsin, centrifuged 600 g for 10 minutes, and washed again with 10 mL of Tyrode (no Ca^{2+} added). The cell pellet was suspended in 0.110 mL of respiratory medium (potassium gluconate 0.14 mM, potassium phosphate 0.005 mM, and digitonin 0.04 μM, Fluo-4 0.001 μM, hepes 0.02 pH 7.1). For the final free Ca^{2+} measurement, 0.1 mL was transferred into p96 wells to register the extramitochondrial free Ca^{2+} (F0 value) using the Synergy HT

microplate reader (λex490 nm/λem530 nm). The intramitochondrial Ca^{2+} content was released by uncoupling with 1 μM carbonyl cyanide-p-trifluoromethoxyphenylhydrazone (FCCP) (F value), and the free Ca^{2+} signal was calibrated with 100 μM $CaCl_2$ and 1 mM EGTA to obtain the Fmax or Fmin values, respectively. The intramitochondrial free Ca^{2+} content was calculated using the equation:

$$\left[Ca^{2+}\right] = K(F - Fmin)/(Fmax - F)$$

where K is the Kd value for the Fluo-4 potassium salt (335 nM). Total protein was determined using the Lowry method with the remaining sample (10 uL), and all data were finally expressed as $[Ca^{2+}]$.

MITOCHONDRIAL DENSITY. Cells were seeded in coverslips and loaded with 1 μM calcein-AM for 30 minutes at 37 °C in Tyrode solution (TS), washed with PBS, then loaded with tetramethylrhodamine ethyl ester perchlorate (TMRE) 300 nM (Thermo Fisher Scientific) during 30 minutes at RT and darkness. Afterward, cells were rinsed with fluorophore-free TS and placed in a recording chamber. CSA 1 μM was added to prevent mitochondrial membrane depolarization and loss of TMRE fluorescent signal, as TMRE is a dynamic fluorescent reporter for membrane potential (ΔΨ) in metabolic active mitochondria. Carbonyl cyanide m-chlorophenyl hydrazone (CCCP) 0.8μM was added at the end of each experiment as a negative control for TMRE staining as it depolarizes the mitochondrial membrane and induces loss of TMRE fluorescent signal.

Fluorescent XY images were acquired using a Leica TCS SP5 confocal microscope equipped with a D-apochromatic 40X, 1.2 NA, oil objective. Calcein excitation was induced using a 488-nm laser, and the emission was detected at 517 nm with a bandwidth of 10 nm. TMRE excitation was induced using a 543-nm laser, and emission was acquired at 580 nm with a bandwidth of 20 nm. Acquired images for calcein and TMRE staining were processed and analyzed using ImageJ software (NIH). Calcein staining was used to assess cell area and TMRE staining was converted into a binary image to assess mitochondrial density.

PROTEIN PURIFICATION AND WESTERN BLOT. Cells were detached and lysed in radioimmunoprecipitation assay (RIPA) buffer (Tris 50 mM, pH 7.5, EDTA 5 mM, NaCl 150 mM, Triton X-100 1%, sodium dodecyl sulfate 0.1%, sodium fluoride10 mM, sodium deoxycholate 0.5%) supplemented with phosphatase and protease inhibitor cocktails (Roche). Lysates were frozen and thawed twice in 3 cycles. Then, the homogenate was centrifuged (2,000 rpm, 10 minutes at 4 °C), and the protein was recovered and quantified by the Lowry method. BSA was used as standard. All protein extracts were stored at -80 °C until analysis.

Proteins were resolved on sodium dodecyl sulfate - polyacrylamide gel electrophoresis, and transferred onto a polyvinyl difluoride membrane. After incubation with primary antibody O/N at 4 °C on a rotating table, the membrane was washed 3 times for 10 minutes with PBS Tween20 0.5%. A horseradish peroxidase-conjugated secondary antibody was incubated for 2 hours at 25 °C; after washing 3 times with PBS 0.5% Tween 20 for 10 minutes, the chemiluminescence signal was detected using EC detection (ThermoFisher) as reagent, and by BioSpectrum 415 Image Acquisi-tion System (UVP). Chemiluminescence was analyzed using Image J software 1.50a (see Supplemental Table 1 for antibody information)

QUANTITATIVE REVERSE TRANSCRIPTASE PCR. Total RNA was obtained after treatment using TRIzol Reagent (15596026, Invitrogen). The purity of all samples was confirmed by measuring their 260/280-nm absorbance ratio using a Take3 multi-volume plate in a Synergy HT microplate reader (BioTek Instruments). RNA integrity was evaluated on a denaturing agarose gel. The cDNA was reverse-transcribed from 1 μg of total RNA using the SensiFAST cDNA Synthesis Kit (BIO-65053, Bioline). The quantitative PCR reaction was performed using the SensiFAST SYBR Lo-ROX Kit (BIO-94020, Bioline) in a QuantStudio 3 System (Thermo Fisher Scientific), and the data were analyzed by the Delta-Delta CT method to estimate each gene's mRNA expression. The primers were synthesized by T4 Oligo. All primer sequences for B-type natriuretic peptide (Nppb), collagen I (Col1a1), transforming growth factor β (Tgfb1), interleukin 6 (Il6), troponin C, MCU, MICU1, MICU2, EMRE, and hypoxanthine-guanine phosphoribosyltransferase (Hprt) as housekeeping are detailed in Supplemental Table 2.

STATEMENT OF ETHICS. Subjects provided written informed consent. The study protocol has been approved by the research institute's committee on human research (protocol number IRB(3N)0511-0100).

STATISTICAL ANALYSIS. Statistical data are presented as mean ± SEM. Comparisons between 2 groups were made using Mann-Whitney U or Student's *t*-test, while Kruskal-Wallis or one-way analysis of variance (ANOVA) followed by a Dunn's post hoc test for multiple pairwise comparisons was used when comparing >2 groups dependent on data distribution. Two-way ANOVA followed by a Sidak post

hoc test was used to compare 2 or more variables between groups; and repeated measurements ANOVA was used to analyze longitudinal data. Comparisons within group were performed using a paired t-test. The Shapiro-Wilk test was used to determine the normal distribution of data. Nonparametric, 2-tailed Spearman r test with a 95% CI was used to analyze correlations. A nonparametric Friedman's ANOVA test was used to analyze repeated measurement in time.

Differences were considered significant when $P < 0.05$. For the normalized fibrotic index and myocyte size, the data were normalized compared to the control's mean. Data processing, graphs, and statistical analysis were performed with GraphPad Prism (V.8).

RESULTS

SILENCING MCU PREVENTS PATHOLOGIC HYPERTROPHY. Studies using animal models to assess the involvement of MCU in acute and chronic conditions of increased workload and pathologic hypertrophy revealed the importance of MCU for cardiac adaptation upon physiological stress.[8,13,22] To elucidate the role of MCU in the underlying mechanisms of energetic dysfunction and hypertrophy in cardiac disease, we studied a widely used model of ANGII-induced mitochondrial dysfunction and hypertrophy in rat cardiac ventricle myocyte H9C2 cells[23] with silenced MCU.

The silencing strategy resulted in a partially downregulated MCU, 46% ($P = 0.037$) at the protein level (Supplemental Figure 1A). This was also validated by immunofluorescence analysis of transfected cells' green fluorescent protein (GFP) expression (transfection fluorescent reporter) and MCU expression (Supplemental Figure 1B). A deeper analysis revealed no MCU positive staining within GFP-positive cells ($P \leq 0.001$) (Supplemental Figure 1C). Silenced cells (shMCU) were characterized by a decreased mCa^{2+} uptake (64% decreased; $P = 0.023$) when compared with cells transfected with a non-coding plasmid (shMock) (Supplemental Figures 1C and 1D). Consequently, the reduced Ca^{2+} entry rate also reflected a reduced mCa^{2+} content ($P = 0.001$) (Supplemental Figure 1E); however, this reduction did not impair ATP content, oxidative phosphorylation, or cell viability (Supplemental Figures 1G to 1I).

Exposure of cells to ANGII resulted in the upregulation of MCU in shMock cells, with 44% increase ($P = 0.034$) at the protein level and 61% ($P = 0.043$) at the mRNA level (**Figures 1A and 1B**). However, ANGII could not shift MCU expression in shMCU cells. Remarkably, shMCU cells showed incapacity to undergo hypertrophy ($P = 0.01$) under ANGII exposure, whereas shMock cells exhibited a 2.3-fold increase ($P = 0.002$) in their area (**Figures 1C and 1D**). This antihypertrophic feature was also observed in transfected cells exposed to isoproterenol (ISO) ($P = 0.039$) (Supplemental Figure 2), where hypertrophy was prevented in shMCU + ISO cells, when compared to shMock + ISO. In addition, at gene expression level, hypertrophic markers BNP ($P = 0.045$) and collagen 1 ($P = 0.047$), as well as proinflammatory markers TGFβ ($P = 0.053$) and IL-6 ($P = 0.043$) (**Figure 1E**) remain unaltered in shMCU cells whereas its upregulation was observed in shMock + ANGII. In addition, the findings in ventricular cardiomyoblasts were evaluated in neonatal cardiomyocytes silenced for MCU and exposed to ANGII (siMCU + ANGII); after 24 hours of exposure, the absence of MCU prevented cell hypertrophy ($P = 0.002$) whereas cardiomyocytes transfected with non-targeting siRNA (scramble + ANGII) presented a 45% increase in cell area ($P = 0.023$) (**Figure 1F**). Also, cell hypertrophy was assessed by visualization of sarcomeric organization,[24] assessed by the recording of the fluorescence intensity profile of sarcomere marker phalloidin Rhodamine (**Figure 1G**). Accordingly, the modification of intensification of fluorescence profiles, which is a trademark of neonatal cardiomyocyte hypertrophy,[24] were corroborated in scramble + ANGII and prevented in siMCU + ANGII (**Figure 1G**). These results revealed the potential role of MCU in the signaling pathway of ANGII related cardiac pathologic hypertrophy.

SILENCING MCU PREVENTS mCa^{2+} OVERLOAD AND mROS GENERATION IN CELLS UNDER PATHOLOGIC HYPERTROPHIC CONDITIONS. We assessed the mitochondrial CRC of permeabilized cells. We observed that ANGII induced a reduction in mCa^{2+} buffering, leading to an early opening of the mPTP in shMock cells, whereas shMCU cells showed protected and increased capacity to retain Ca^{2+} at 2.7-fold ($P = 0.030$) higher than that of shMock cells (**Figures 2A and 2B**). We found that ANGII dose-dependently lowered CRC in shMock cells, whereas shMCU cells were able to retain more mCa^{2+} ($P = 0.009$) (**Figure 2C**). These observations can be explained by the fact that, under the ANGII stimulus, shMock cells possess upregulated MCU and, therefore, an increased mCa^{2+} content. In fact, shMock cells stimulated with ANGII presented a 3.3-fold increase in mCa^{2+} content compared to shMCU cells ($P = 0.0274$) (**Figure 2D**). This suggests that, in

FIGURE 1 **Silencing MCU Prevents Pathologic Hypertrophy**

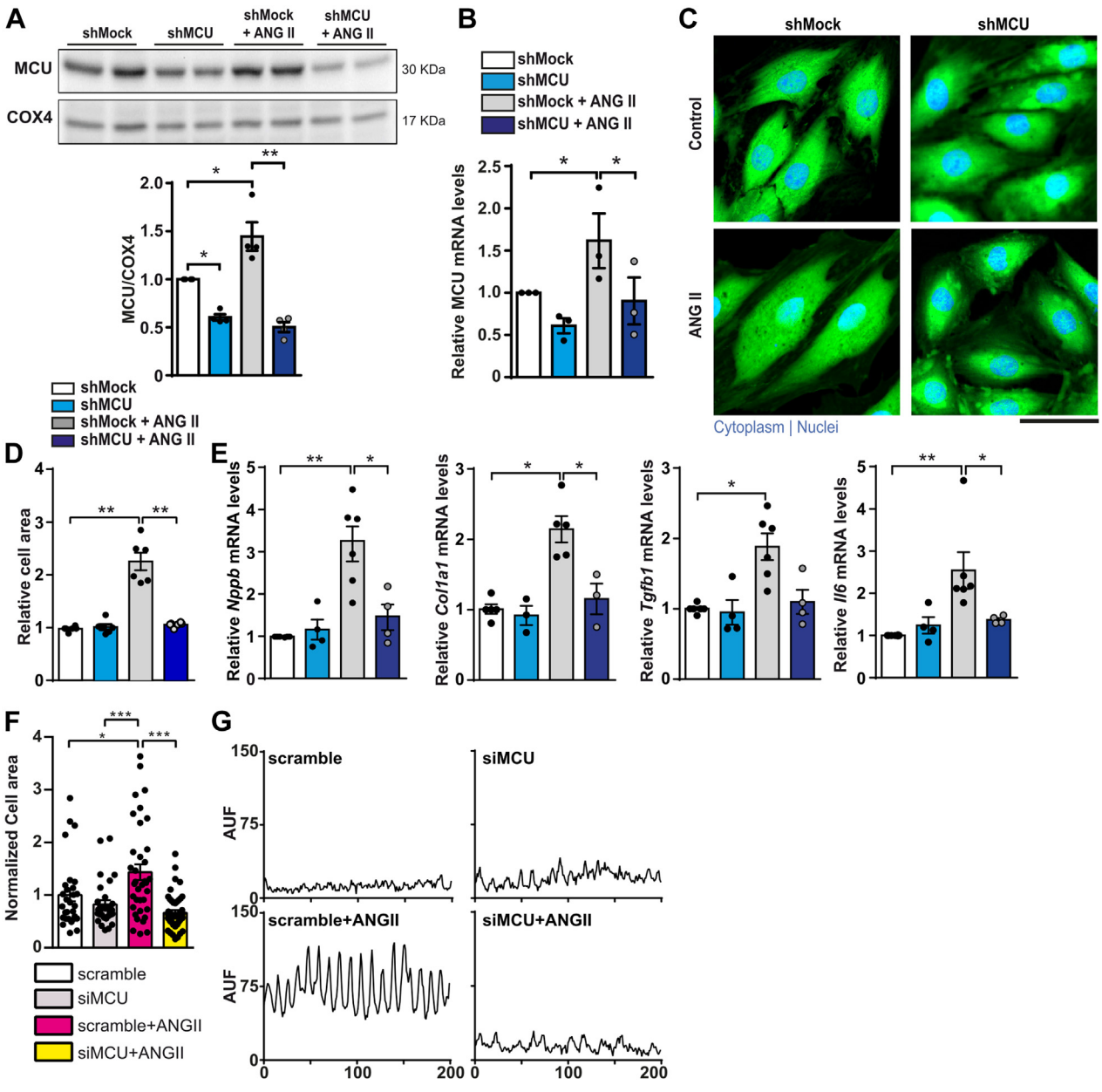

Mitochondrial calcium uniporter (MCU) was downregulated by transfecting H9C2 cells with a short hairpin RNA (shRNA) – green fluorescent protein (GFP) against MCU (shMCU) but not a nonspecific scramble shRNA-GFP (shMock). ShMCU and shMock were cultured under chronic angiotensin II (ANGII)–induced hypertrophy conditions: 1 μM ANGII for 48 hours. (A) Representative blot image (top) and semiquantification (bottom) of the protein level of MCU assessed by Western blotting in cell lysates (n = 4). (B) Relative mRNA levels of MCU (n = 3). (C) Representative fluorescent images of hypertrophy. Images acquired with fluorescent confocal microscopy. Cell hypertrophy was evaluated by assessing cell area using cytoplasmic fluorescent staining by calcein; nuclei were stained using DRAQ5; scale bar 50 μm. (D) Semi-quantification of cell area as stained by calcein (n = 100 cells × 6 experiments). (E) Relative gene expression of remodeling gene markers B-type natriuretic peptide (*Nppb* gene), collagen type 1 (*Col1a1* gene), and proinflammatory gene markers tumor growth factor β 1 (*Tgfb1* gene) and interleukin 6 (IL-6) (*Il6* gene). (F) Relative semiquantitative cell area from cardiomyocytes silenced for MCU and stimulated with ANGII determined from fluorescent images acquired with fluorescent confocal microscopy using cytoplasmic fluorescent calcein staining (n = 4, 35 cells/experiment). (G) Fluorescence densitometric profiles obtained by analyzing a longitudinal section of the cardiomyocyte stained with Phalloidin Rhodamine. Units are arbitrary units of fluorescence (AUF). Statistics: dots represent individual values, and bars represent mean ± SEM. (A to E) Kruskal-Wallis test with Dunn's post hoc test for multiple pairwise comparisons. (F) One-way analysis of variance with Dunn's post hoc. *$P < 0.05$. **$P < 0.01$. ***$P < 0.001$.

FIGURE 2 Silencing MCU Prevents mCa^{2+} Overload and mROS Generation in Cells Under Pathologic Hypertrophic Condition

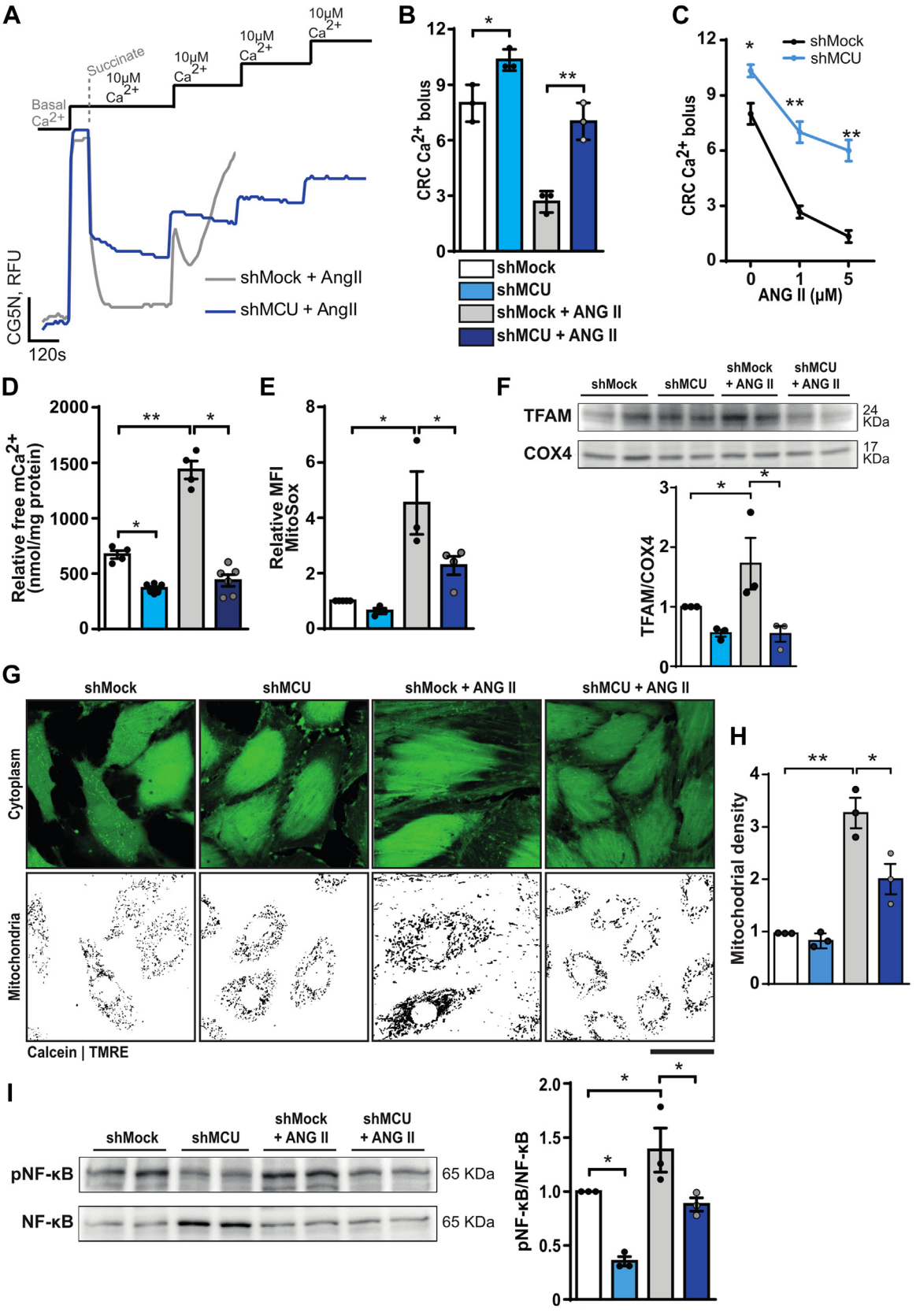

Continued on the next page

hypertrophic cardiac cells, increased MCU expression followed by mCa^{2+} overload drives mitochondria toward $\Delta\Psi$ depolarization and opening the mPTP.

Another key event driven by mCa^{2+}overload is the generation of mROS; previous studies have shown that mCa^{2+} influences the production of mROS.[25] Thus, we explored whether MCU-mediated mCa^{2+} overload upon ANGII exposure affects mROS generation. As shown in **Figure 2E**, upregulation of MCU in shMock increased mROS levels ($P = 0.032$). We also observed increased mitochondrial biogenesis, which could explain the augmented mROS. Here, we found that MCU-mediated mCa^{2+} overload induced by ANGII in shMock cells enhanced the levels of mitochondrial transcription factor (TFAM), is considered a master regulator of mitochondrial biogenesis, and whose increased levels are directly associated with increased mitochondrial DNA[26,27] ($P = 0.027$) (**Figure 2F**). To corroborate this, we assessed mitochondrial density using TMRE staining in the presence of CSA. The results showed that in ANGII-induced mCa^{2+} overload, there was an increase in the mitochondrial density by more than 3-fold ($P = 0.001$), confirming the role of mitochondrial biogenesis in the mCa^{2+}-mediated generation of mROS (**Figures 2G and 2H**). To further understand the role of mROS-induced pathologic remodeling, we reproduced the model by adding mitoTEMPO, an mROS scavenger. This produced a striking effect, as mitoTEMPO, similar to shMCU cells, prevented cell hypertrophy ($P = 0.010$) and, as expected, mROS accumulation ($P = 0.003$) (Supplemental Figures 3A and 3B), revealing the importance of mROS in the mechanism of cell remodeling.

It has been well established that the ROS-activated nuclear factor kappa B (NF-κB) signaling pathway has a tremendous impact on the pathophysiology of HF by promoting the expression of remodeling and proinflammatory markers.[28] In **Figure 2I**, we show that NF-κB activation (phosphorylation) was increased in shMock + ANGII ($P = 0.013$), and as expected, in the absence of MCU, its activation was decreased ($P = 0.050$), showing the direct relationship between MCU-mediated mCa^{2+} overload, mROS generation, and NF-κB activation in the underlying mechanism of cell remodeling.

INHIBITING THE MITOCHONDRIAL NA^+/CA^{2+} EXCHANGER INDUCES MITOCHONDRIAL CA^{2+} OVERLOAD AND REVERTS THE ANTIHYPERTROPHIC EFFECT OF SILENCING MCU. To further clarify the importance of mCa^{2+} overload on the molecular mechanisms of pathologic remodeling, we promoted mCa^{2+} overload in shMCU cells, bypassing the absence of MCU, by using an inhibitor (CGP37157) of the NCLX. Na^+/Ca^{2+} exchange is the primary mechanism for mCa^{2+} extrusion in cardiac cells, and its inhibition thus promotes mCa^{2+} accumulation.[29]

Regarding this, blocking NCLX in shMCU cells exposed to ANGII generated a hypertrophic phenotype, with shMCU + ANGII + CGP (NCLX inhibitor: 7-chloro-5-(2-chlorophenyl)-1,5-dihydro-4,1-benzothiazepin-2(3H)-one) cells presenting an increased cell area 2.3-fold when compared with nonhypertrophic shMCU cells ($P = 0.002$) (**Figure 3A**). Moreover, these cells also showed increased mCa^{2+} content ($P = 0.060$) (**Figure 3B**), followed by a reduced CRC ($P = 0.004$) (**Figure 3C**) and a remarkable increase in

FIGURE 2 Continued

ShMCU and shMock were cultured under chronic ANGII-induced hypertrophy, 1 μM ANGII for 48 hours. (A,B) Mitochondrial calcium (Ca^{2+}) retention capacity (CRC) evaluated fluorometrically with the Ca^{2+} green 5N (CG5N) dye. Cells suspended in a Ca^{2+}-free media were periodically stimulated with 10 μM Ca^{2+} bolus until the opening of the mitochondrial permeability pore (mPTP), releasing the mitochondrial Ca^{2+} (mCa^{2+}) content. Representative recording (A) and semiquantification (B) are shown. (C) Mitochondrial calcium retention captacity (mCRC) in permeabilized shMock and shMCU cells previously exposed to the ANGII-induced hypertrophy at the ANGII concentrations of 1 μM and 5 μM for 48 hours. (D) Free mCa^{2+} release by permeabilized transfected cells. Cells were loaded with Fluo-4 and suspended in a free Ca^{2+} media, followed by exposure to the oxidative phosphorylation uncoupler FCCP to induce ultimately mitochondrial membrane disruption and content release. (E) Production of mitochondrial reactive oxygen species (mROS) assessed by flow cytometry analysis of intracellular MitoSO Red fluorescent staining from live cells. Semiquantitative analysis from fluorescence histograms is shown. (F) Mitochondrial biogenesis assessed by the detection of mitochondrial transcription factor (TFAM) using Western blotting in cells (n = 3); representative blot image and semiquantification are shown. (G,H) Mitochondrial density is assessed by fluorescence analysis of TMRE-positive stained area of each cell, normalized against cell area. Cell hypertrophy was evaluated by assessing cell area using cytoplasmic fluorescent staining by calcein. Representative fluorescent images acquired with fluorescent confocal microscopy; scale bar 50 μm. (I) Activation of reactive oxygen species (ROS) –dependent prohypertrophic and proinflammatory transcription-factor nuclear factor kappa B (NF-κB) assessed by Western blotting in cell lysates from transfected cells (n = 3), representative blot image from NF-κB phosphorylation (pNF-κB) and total NF-κB along with their semiquantitative ratio are shown. Data are presented as mean ± SEM; (A,B,D,E,F,G, and I) 1-way analysis of variance (ANOVA) with Dunn's post hoc test for multiple pairwise comparisons; (C) 2-way ANOVA with Sidak post hoc test. *$P < 0.05$. **$P < 0.01$. ***$P < 0.001$. FCCP = Carbonyl cyanide-p-trifluoromethoxyphenylhydrazone; MFI = median fluorescence intensity; RFU = relative fluorescence units; other abbreviations as in **Figure 1**.

FIGURE 3 Inhibiting the Mitochondrial Na^+/Ca^{2+} Exchanger Induces mCa^{2+} Overload and Reverts Antihypertrophic Effect in Silenced MCU Cells

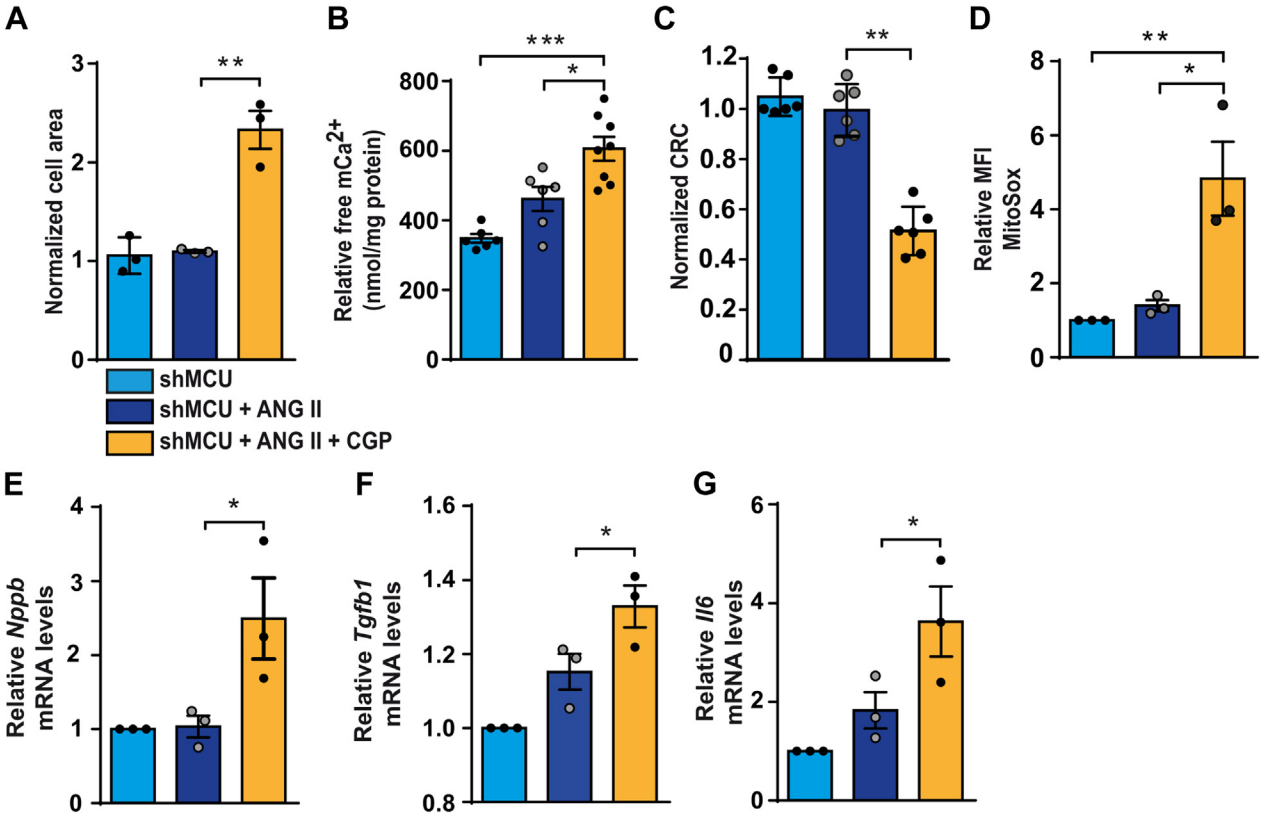

shMCU cells exposed to ANGII-induced hypertrophy (1 μM ANGII, 48 hours) were treated simultaneously with the mitochondrial Na^+/Ca^{2+} exchanger (NCLX) inhibitor CGP37157 at 5 μM. (A) Relative semiquantitative cell area from cells treated with CGP37157 determined from fluorescent images acquired with fluorescent confocal microscopy (n = 3). Cell hypertrophy was evaluated by assessing cell area using cytoplasmic fluorescent calcein stain. (B) Free mCa^{2+} release by permeabilized cells. Cells were loaded with Fluo-4 and suspended in a free Ca^{2+} medium, followed by exposure to the OxPhos uncoupler FCCP to induce mitochondrial membrane disruption and content release (n = 6 to 8). (C) mCRC in permeabilized cells. Relative gene expression of (D) remodeling gene markers B-type natriuretic peptide (*Nppb* gene, n = 3) and proinflammatory gene markers (E) TGFβ 1 (*Tgfb1* gene, n = 3) and (F) IL-6 (*Il6* gene, n = 3). Bars represent mean ± SEM; Kruskal-Wallis test with Dunn's post hoc test for multiple pairwise comparisons. *$P < 0.05$. **$P < 0.01$. ***$P < 0.001$. CGP = CGP37157 a NCLX inhibitor; other abbreviations as in Figures 1 and 2.

mROS generation ($P = 0.014$) (Figure 3D), along with the upregulation of remodeling marker BNP ($P = 0.035$) (Figure 3E) and proinflammatory markers TGFβ ($P = 0.038$) (Figure 3F) and IL-6 ($P = 0.040$) (Figure 3G). These data provide clear evidence that mCa^{2+} overload-induced mROS generation drives pathologic cardiac remodeling. Other attempts were made to induce mCa^{2+} overload and associated cellular hypertrophy in shMCU cells by using MCU activators Kaempferol and Spermine, 2 organic compounds that are known to increase MCU activity.[30] Nevertheless, because of the low expression of MCU, we could not induce changes in the phenotype of shMCU cells (data not shown).

INHIBITING MCU WITH RU_{360} PREVENTS mCa^{2+} OVERLOAD AND ANGII-INDUCED REMODELING. Ru_{360} is a potent MCU inhibitor with relevant results in preventing cardiac injury[10,31] and with potential application in targeting MCU in HF.[11] Therefore, we studied the ability of Ru_{360} to prevent MCU-driven mCa^{2+} overload and cellular remodeling induced by ANGII in shMock cells. Results showed notable prevention of cell hypertrophy by Ru_{360} ($P = 0.016$) (Figure 4A), followed by expected prevention of mCa^{2+} overload ($P = 0.005$) (Figure 4B), and consequent reduced mROS generation ($P = 0.036$) (Figure 4C). This reveals that MCU inhibition by Ru_{360} can serve equally to prevent mCa^{2+}-induced mROS,

FIGURE 4 Inhibiting MCU With Ru_{360} Prevents Mitochondrial Ca^{2+} Overload and Angiotensin-Induced Hypertrophy

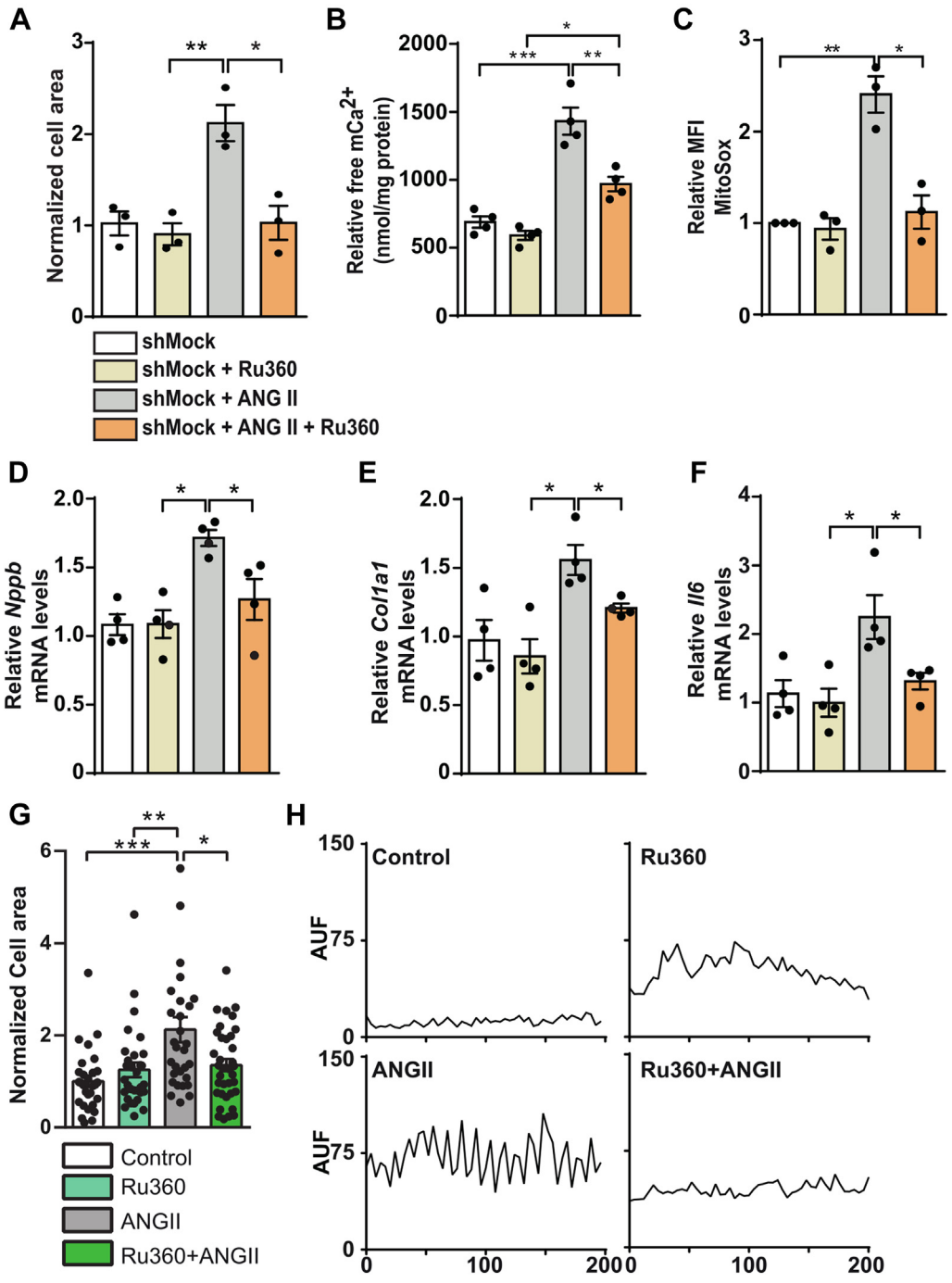

shMCU cells exposed to ANGII-induced hypertrophy (1 μM ANG II, 48 h) were treated simultaneously with the MCU-specific inhibitor ruthenium 360 (Ru_{360}) at 1 μM. (A) Relative semiquantitative cell area of cells treated with ANGII and Ru_{360} determined from fluorescent images acquired with fluorescent confocal microscopy (n = 3). Cell hypertrophy was evaluated by assessing cell area using cytoplasmic fluorescent calcein stain. (B) Free mCa^{2+} release by permeabilized cells. Cells were loaded with Fluo-4 and suspended in a free Ca^{2+} medium, followed by exposure to the OxPhos uncoupler FCCP to induce mitochondrial membrane disruption and content release (n = 4). (C) Production of mROS assessed by flow cytometry analysis with intracellular MitoSOX Red fluorescent staining from live cells (n = 3). Relative gene expression of (D) remodeling gene markers B-type natriuretic peptide (*Nppb* gene, n = 4) and collagen type 1; (E) (*Col1a1* gene, n = 4); and (F) proinflammatory gene marker IL-6 (*Il6* gene, n = 4). (G) Relative semiquantitative cell area from cardiomyocytes exposed to Ru_{360} and stimulated with ANGII (n = 4, 35 cells/experiment), and (H) corresponding fluorescence densitometric profiles. Dots represent individual values and bars represent mean ± SEM. (A to F) Kruskal-Wallis test with Dunn's post hoc test for multiple pairwise comparisons. (G) One-way ANOVA with Dunn's post hoc test. *$P < 0.05$. **$P < 0.01$. ***$P < 0.001$. Abbreviations as in Figures 1 and 2.

FIGURE 5 ANGII Induces MCU Upregulation Through a Ca^{2+}-Dependent CAMKII/CREB Activation Signaling

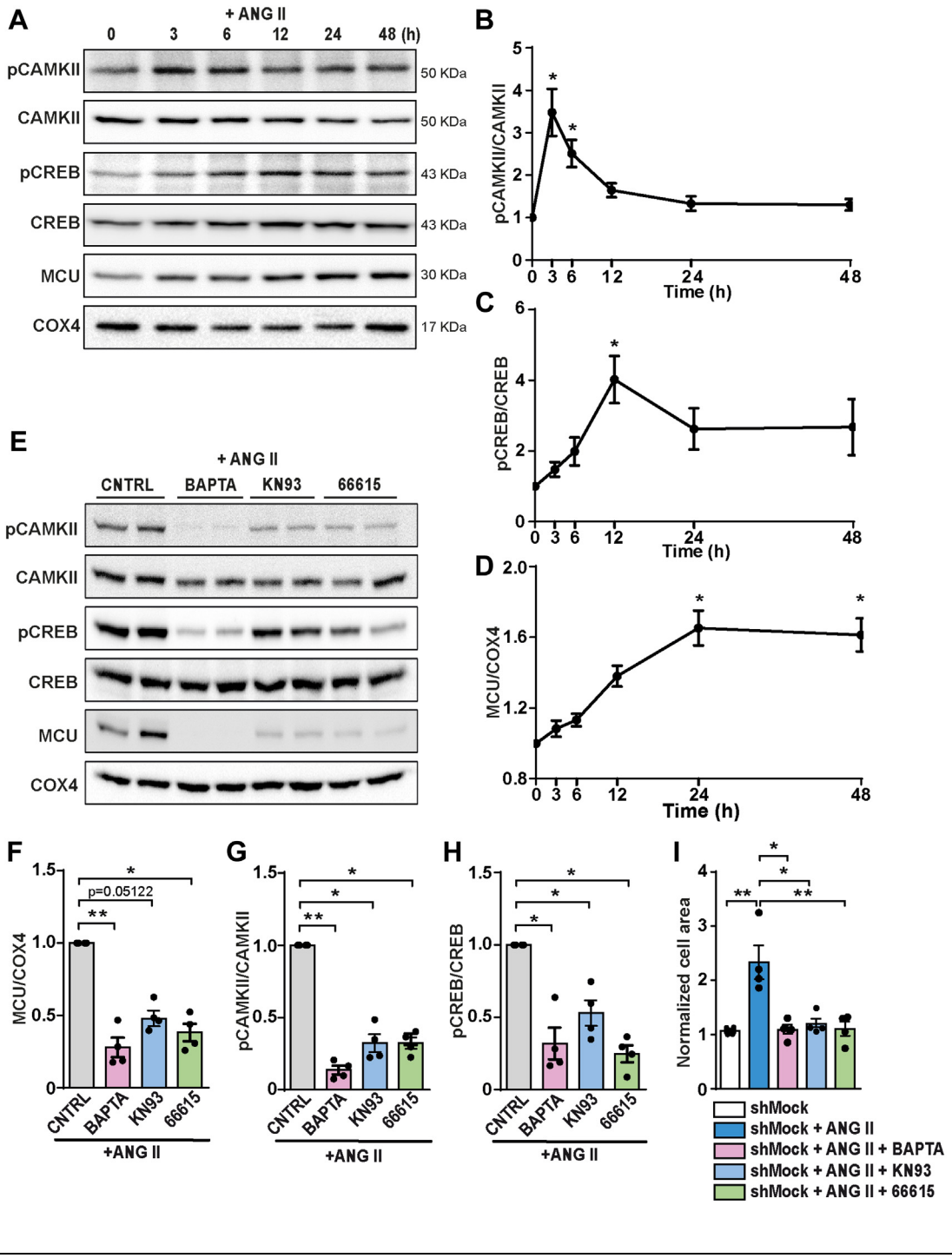

Continued on the next page

as previously seen with shMCU cells. Because of this effect, we also observed downregulation of remodeling markers BNP ($P = 0.041$) (Figure 4D) and collagen 1 ($P = 0.043$) (Figure 4E), along with reduced proinflammatory marker IL-6 ($P = 0.049$) (Figure 4F). This finding unveils a potential pharmacologic approach to inhibit MCU activity and prevent cellular injury and remodeling. In this sense, MCU activity was blocked in neonatal cardiomyocytes with Ru_{360}. Results confirmed that Ru_{360} can prevent ANGII-induced increased cell area ($P = 0.012$) (Figure 4G) and sarcomere organization in cardiomyocytes (Figure 4H), leading Ru_{360} a step forward in the validation process as a new pharmacologic approach to treat heart hypertrophy.

ANGII INDUCES MCU UPREGULATION THROUGH A CA^{2+}-DEPENDENT CAMKII/CREB SIGNALING. We explored the molecular mechanisms by which the upregulation of MCU can induce mitochondrial dysfunction and cardiac remodeling. However, one question remains to be solved to complete the puzzle: What is the mechanism of MCU upregulation by ANGII? In a Ca^{2+}-dependent manner, transcriptional activation of CREB is known to bind directly to the MCU promoter, inducing gene expression.[32] Therefore, we studied the MCU expression pathway via the ANGII receptor downstream activation of CREB[32] and how its activation is mediated by CAMKII.[33] We performed a time-course phosphorylation of CREB and CAMKII by ANGII in shMock cells (Figure 5A). In this context, we observed that ANGII induced early transient activation of CaMKII, with peak activity at 3 hours ($P = 0.002$) (Figure 5B), followed by a maximum activation of CREB at 12 hours ($P = 0.003$) (Figure 5C), and a sustained but reduced phosphorylation level until 48 hours. By comparison, the MCU protein levels reached maximum expression at 24 hours ($P = 0.01$) (Figure 5D). Further, MCU activity was measured by assessing mCa^{2+} influx to study MCU early posttranslational modification driven by ANGII and early activation of CAMKII, which could contribute to an increased mCa^{2+} overload. However, no differences were found at the determined maximum time point of CAMKII activity at 3 hours, or even at 6 hours, which could indicate altered MCU activity (Supplemental Figures 4A and 4B).

To validate the involvement of CREB and CAMKII activity in MCU expression, we exposed cells to selective CREB and CAMKII activity inhibitors, 66615 and KN93, respectively, for 48 hours. As shown in Figure 5E, the blot and subsequent semiquantifications showed a remarkable correlation with CAMKII-mediated CREB activation, in which KN93 inhibited the phosphorylation of CAMKII and CREB (Figures 5E and 5G show KN93 with $P = 0.037$; and 66615 with $P = 0.049$; and Figure 5H shows KN93 with $P = 0.016$; and 66615 with $P = 0.021$). Remarkably, both inhibitors were able to dramatically reduce MCU protein levels, revealing a strong regulation of MCU by CREB/CAMKII signaling (Figures 5E and 5F) (KN93: $P = 0.013$; 66615: $P = 0.021$). CAMKII activation was also impacted by 66615 (Figures 5E and 5G), revealing a potential long-term effect of CREB inhibitor in overall CAMKII activation, such as changes in mROS, one known activator of CAMKII, or changes in intracellular Ca^{2+} dynamics, all driven by downregulation of MCU and mROS-mediated mCa^{2+} overload.

We observed that phosphorylation of CAMKII and CREB, as well as MCU expression, were severely diminished in the presence of BAPTA (2,2′,2″,2‴-[Ethane-1,2-diylbis(oxy-2,1-phenylenenitrilo)]tetraacetic

FIGURE 5 Continued

The mechanisms underlying MCU upregulation upon chronic exposure to prohypertrophic ANGII were evaluated in shMock cells. (A) Time-course activation of Ca^{2+}/calmodulin-dependent protein kinase II (CAMKII) and cyclic adenosine monophosphate response element-binding protein (CREB) and upregulation of MCU were assessed by Western blotting (WB), using cell lysates from shMock obtained 3, 6, 12, 24 and 48 hours posterior to the exposure of 1 μM ANGII. Representative blot images are shown from phosphorylated CAMKII, vs total CAMKII phosphorylated CREB vs total CREB, MCU vs COX4 expressions for the same WB membrane. (B) Semiquantification for the time-course activation of CAMKII by ANGII, determined by the relation between phospho-CAMKII and total-CAMKII (n = 4). (C) Semiquantification for the time-course activation of CREB by ANGII determined by the relation between phospho-CREB and total-CREB (n = 4). (D) Semiquantification for the time-course upregulation of MCU by ANGII normalized for COX4 expression (n = 4). (E) Activation of CAMKII and CREB and expression of MCU in shMock cells cultured in the presence of 1 μM ANGII and 5 μM BAPTA-AM (Ca^{2+} chelator), or 5 μM KN93 (CAMKII inhibitor), or 1 μM 66615 (CREB inhibitor) for 48 hours assessed by WB. Representative image obtained from the same membrane. (F,G,H) Semiquantification for WB detection of the MCU expression vs COX4 (n = 4) (F), phospho-CAMKII vs total-CAMKII (n = 4) (G), and phospho-CREB vs total-CREB (n = 4) (H) determined for shMock cells cultured in the presence of BAPTA, KN93, and 66615. (I) Inhibiting Ca^{2+}/CAMKII/CREB signaling prevents cell hypertrophy. shMock were cultured in the presence of 1 μM of ANGII and 5 μM BAPTA-AM, or 5 μM KN93 or 1 μM 66615 for 48 hours. Relative semiquantitative cell area was determined from fluorescent images acquired with fluorescent confocal microscopy (n = 4). Cell hypertrophy was evaluated by assessing cell area using cytoplasmic fluorescent staining by calcein. Data are presented as mean ± SEM. (B to D) Show 1-way repeated measures ANOVA and (E to H) show 1-way ANOVA with Dunn's post hoc test for multiple pairwise comparisons. *$P < 0.05$. **$P < 0.01$. ***$P < 0.001$. BAPTA-AM = membrane-permeable form of BAPTA: 1,2-Bis(2-aminophenoxy)ethane-N,N,N′,N′-tetraacetic acid tetrakis(acetoxymethyl ester; other abbreviations as in Figures 1 and 2.

FIGURE 6 MCU Overexpression is Associated With ANGII-Induced Heart Hypertrophy and HF

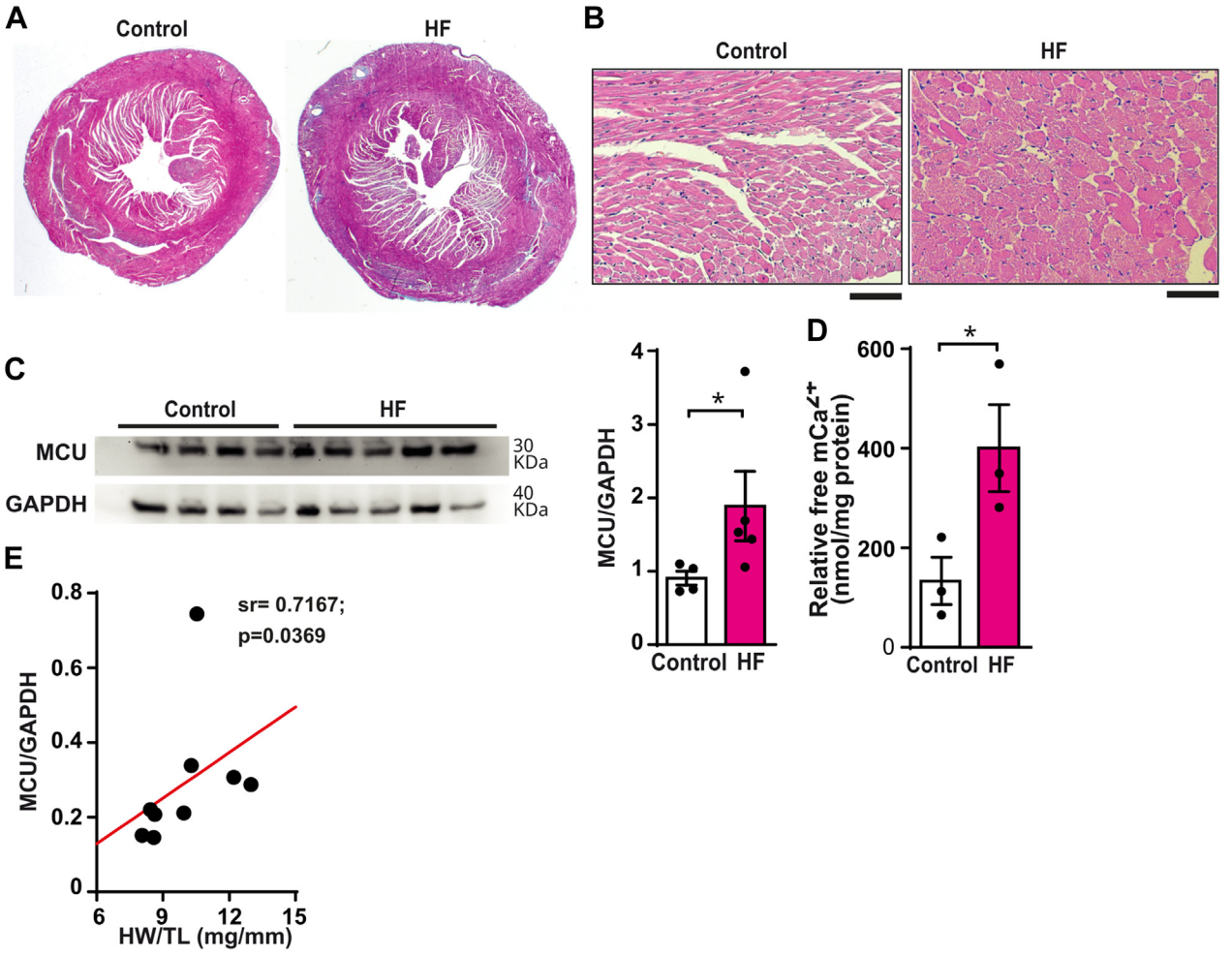

(A) Representative micrographs of cardiac tissue: Masson's trichrome stain to visualize fibrotic areas, original magnification ×1.25 (n = 6). (B) Hematoxylin and eosin (HE) stain for cardiac myocyte area assessment, original magnification ×10 (n = 6). (C) Representative blot image (top) and semiquantification (bottom) of the protein level of MCU assessed by WB in cell lysates (n = 5). (D) Free mCa^{2+} release by permeabilized cardiomyocytes, loaded with Fluo-4 and suspended in a free Ca^{2+} medium. (E) Spearman correlation analysis between MCU protein levels normalized to glyceraldehyde 3-phosphate dehydrogenase (GAPDH) and heart weight normalized with tibia length. Data are presented as mean ± SEM and Mann-Whitney with post hoc Tukey's multiple comparisons test. *$P < 0.05$. **$P < 0.01$. HF = heart failure; HW = heart weight; TL = tibia length; other abbreviations as in Figures 1, 2, and 5.

acid), a Ca^{2+} chelator, revealing strong and dependent regulation of these by intracellular Ca^{2+} (Figures 5E to 5H). Therefore, we studied how these inhibitors could impact MCU/mCa^{2+} overload-dependent cell remodeling by analyzing the cell area in the presence of ANGII in shMock cells. The results in Figure 5I clearly showed that cell hypertrophy was prevented in the presence of BAPTA ($P = 0.014$), KN93 ($P = 0.016$), and 66615 ($P = 0.007$). Considering these, we could define a Ca^{2+}-dependent CREB/CAMKII regulatory signaling that mediates MCU overexpression and pathologic hypertrophy induced by ANGII.

MCU OVEREXPRESSION IS ASSOCIATED WITH ANGII-INDUCED HEART HYPERTROPHY AND HF. In response to the previous results, it is important to understand the impact of ANGII-induced MCU expression and mCa^{2+} overload in the development of HF. Thus, LVs from mice with HF with reduced ejection fraction (EF) and cardiac hypertrophy were analyzed. HF was induced by chronic exposure to ANGII. The structural effect of ANGII in HF was evaluated. Representative slides of Mason's trichrome and HE stain showed an increase in cardiac fibrosis and myocyte area (Figures 1A and 1B),

followed by an impairment in heart steady-state hemodynamic parameters with reductions in stroke volume ($P = 0.003$), and EF ($P = 0.012$) (Supplemental Table 3), measured by intraventricular-PV Loops measurements. Additionally, MCU protein was overexpressed in HF ($P = 0.0317$) (**Figure 6C**), resulting in increased mitochondrial Ca^{2+} content from isolated cardiomyocytes ($P = 0.048$) (**Figure 6D**). Remarkably, MCU overexpression was also positively correlated with heart weight (r = 0.717) (**Figure 6E**). This represents a direct association between MCU expression and heart hypertrophy, where mitochondrial calcium overload-mROS are a driving pathologic force in the hypertrophic mechanism induced by ANGII.

MCU OVEREXPRESSION IS ASSOCIATED WITH THE PATHOLOGIC REMODELING IN HUMAN HF. Characterizing the failing human heart is fundamental to understanding the molecular changes that occur and that can be correlated with the phenotype of the disease. Following the observations made in our model of ANGII-induced heart hypertrophy, it is likely that changes in MCU expression can occur in the failing human heart as an adaptive response related to mitochondrial dysfunction and potentially to the pathologic remodeling that characterizes HF. To test this notion, LV samples were collected during cardiac transplantation from patients suffering from nonischemic heart disease with a reduced EF (Heart failing left ventricle [HF-LV] 20.2% ± 10.6% vs Non-failing left ventricle [NF-LV] 59.5% ± 13.7%; $P < 0.0001$) and a significant increase in end-diastolic (1.88-fold; $P < 0.0001$) and end-systolic (2.9-fold: $P < 0.0001$) dimensions, which reflect ventricle enlargement-hypertrophy-remodeling, and progressive LV insufficiency.[34] For more details on demographics and population characterization, please see Supplemental Table 4.

Accessing gene and protein expression within these samples by immunohistochemistry and quantitative reverse transcriptase (qRT) PCR, we found an upregulation of MCU (38% by immunohistochemistry, $P = 0.031$; and a 5.9-fold increase by qRT-PCR, $P = 0.0253$) in the LV from failing human heart (**Figures 7A to 7C**). Notably, 96% of the samples presented upregulation of MCU, and only in 1 patient with HF a lower transcript level was found when compared with non-failing LVs (**Figure 7C**). This shows that MCU upregulation is consistent with the pathophysiology and development of the disease. Furthermore, we observed a correlation between MCU upregulation and severity of disease, with MCU transcript level negatively correlated with EF from LV (r = −0.5939) (**Figure 7D**) and positively correlated with LV dimensions and hypertrophy (left ventricular end-systolic dimension: r = 0.5547; left ventricular end-diastolic dimension: r = 0.5577) (**Figure 7D**). These findings provide evidence of a potential relationship between negative feedback in LV molecular plasticity in HF and MCU expression, indicating that the associated energy supply could be linked with cardiac remodeling and declined cardiac function. In this regard, the most striking result that supports this hypothesis was the downregulation of MCU expression in patients with HF who received an LVAD implantation to reduce heart workload and energetic demand ($P = 0.041$), showing a clear capacity of the heart to modulate MCU expression in response to its energetic necessities (**Figure 7E**).

DISCUSSION

HF creates an enormous burden on patient health and health care systems. However, it is a complex disease, and its pathophysiology is still not fully understood. To elucidate key pathways and targets that can potentially change disease and treatment paradigms, this study identified a key mechanism driving cell hypertrophy and mitochondrial dysfunction by mCa^{2+} overload through the upregulation of MCU. In the present study, such mechanism was studied first in a cell line of rat myoblasts, and second in isolated rat cardiomyocytes followed by translation results in LVs from a mouse model of ANGII-induced HF. Two main experimental designs were tested: (1) ANGII-induced hypertrophy and MCU loss of function by siRNA and shRNA, and (2) pharmacologic inhibition using Ru360. Finally, the translation of these findings was corroborated in LVs from failing human hearts, expanding the role of the MCU in the physiopathology of HF's hypertrophy.

A correct mCa^{2+} handling is fundamental for cardiac work,[35,36] and this study shows the importance of mCa^{2+} and MCU in the development of pathologic hypertrophy. Our findings reveal that MCU expression is linked with human HF pathologic remodeling and cardiac work impairment by correlating negatively with EF and positively with left ventrice systolic and diastolic dimensions. Strikingly, after LVAD implantation, the downregulation of the MCU was observed, consistent with the reported lessening of cardiac remodeling and pressure overload induced by the device.[37] Therefore, this shows the metabolic plasticity of the heart by modifying the expression of crucial proteins involved in metabolism, such as MCU, to cope with energy demand, supporting the

FIGURE 7 MCU Overexpression is Associated With Pathologic Remodeling in Human HF

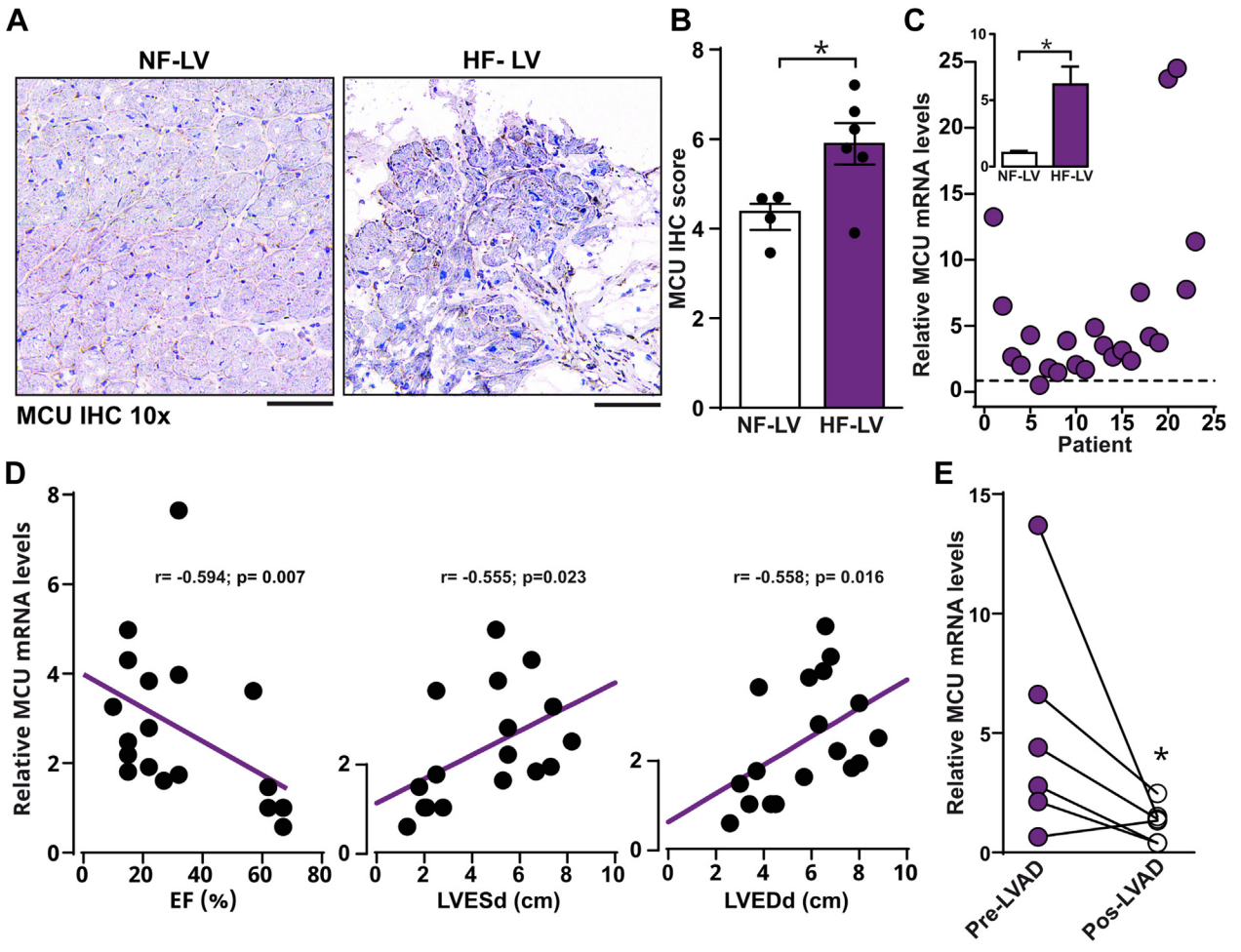

(A, B) Immunohistochemical (IHC) analysis of left ventricular (LV) cryosections from nonfailing (NF-LV) and heart failure (HF-LV). Original magnification ×10x. Scale bar = 500 μm. (C) Relative mRNA levels (quantitative reverse transcriptase polymerase chain reaction) of *MCU* in LV samples from HF-LV patients in relation to NF-LV normalized (dash line, value = 1). The inner bar chart represents relative average ± SEM *MCU* mRNA expression between NF-LV and HF-LV patients. (D) Spearman correlation analysis between *MCU* mRNA levels and the hemodynamic parameters of ejection fraction (EF) (left), left ventricular end-systolic dimension (LVESd) (center), and left ventricular end-diastolic dimension (LVEDd) (right) using Spearman rank correlation test. Each point represents a patient; the purple line represents the Spearman trendline, Sr (Spearman correlation coefficient) and probability value (*P*) were determined for each correlation. (E) Relative *MCU* mRNA levels from LV samples obtained from patients with HF who underwent surgical implantation of a left ventricular assist device (LVAD). The graph shows *MCU* mRNA levels before (purple) and after (white) LVAD implantation for each patient. Each dot represents 1 patient. Data are presented as mean ± SEM. B and C use the unpaired t-test and E uses the paired t-test. *$P < 0.05$. Abbreviations as in Figures 1 and 6.

idea of metabolic and molecular adaptation of the tissue or cells through matching energetic supply to demand.

The role of MCU in the development of HF is still debated regarding the best approach for treating cardiovascular dysfunction: inhibiting or promoting MCU activity. Studies such as ours and others[13,38,39] display data that agree on downregulating MCU activity to prevent mitochondrial Ca^{2+} overload and thus mitochondrial dysfunction and disease progression. However, 2 studies report that upregulating MCU could be beneficial.[40,41] Although contradictory, there are a few points worth mentioning. First, both studies state that the benefits are observed when mCa^{2+} concentration is maintained in control levels, which agrees with our findings. Liu et at[40] found benefit in overexpressing MCU to return to baseline levels, as they observed a slower slope in

mitochondrial Ca^{2+} uptake and decreased mCa^{2+} accumulation. Wang et al[41] used germline MCU knockout mice to test the effects of MCU inhibition on chronic B-adrenergic stimulation. This may have some translational problems because mice with altered germline mCa^{2+} transport seem to show different physiological adaptations in contrast to acute inhibition of mCa^{2+} transport. Such difference is evidenced by mice expressing a dominant negative form of MCU, which shows no mCa^{2+} transport but confers no protection against ischemia reperfusion.[42] By contrast, in an inducible adult cardiomyocyte-specific MCU deletion model, this conferred protection against such injury.[3] Wang et al[41] also briefly tested the effects of MCU inhibition with a model similar to that used by Kwong et al[3], although some caveats arise. It is known that homozygous αMHC-MerCreMer may develop spontaneous focal fibrosis and depressed LV function upon tamoxifen treatment, which may introduce confounders when assessing cardiovascular dysfunction.[43,44] Likewise, the model used suggests having a completely abolished mCa^{2+} transport at the point when the therapeutic window for beneficial mitochondrial transport inhibition is achieved with just a modest inhibition, which again restores mCa^{2+} oscillations similar to control conditions.[45] As to why there is a difference in mCa^{2+} uptake when compared to our model, there could be differing physiological adaptations in different causes of cardiac disfunction and the clinical stages at which this dysfunction is measured. Changes in stoichiometry or post-translational modifications cannot be ruled out as a cause for different Ca^{2+} uptake patterns. Michels et al[46] reported different pharmacologic responses in Ca^{2+} currents between mitoplasts from failing and non-failing hearts[46] with reduced channel activity in failing hearts, although the decreased activity may be partly due to a decline in mitochondrial membrane potential, the driving force for Ca^{2+} transport. In a clinical study, Paillard et al[47] did not find differences in MCU expression but rather MICU1 and MICU2, although the samples came mainly from patients with ischemic and idiopathic HF (having only 3 patients with non-ischemic HF) as opposed to our cohort comprised entirely of patients with nonischemic HF. Even within the same cohort, ischemic and idiopathic patients exhibited significant differences, showing that the underlying etiology of HF must be considered. Although there may be differences in the expression of the different MCU components between studies (probably due to different etiologies and clinical stages), the end goal of preserving mitochondrial Ca^{2+} uptake and concentration is always the same, which only highlights the importance of continuing to study the effects of mCa^{2+} transport in cardiac dysfunction for its potential as a therapeutic target to prevent or treat HF.

Our study is supported by several other studies.[3,8,13,38] In a pressure-overload mouse model of aortic constriction, Ge et al[38] showed that upregulation of MCU, together with heart hypertrophy, increased diastolic and systolic dimensions, reduced EF, and increased expression remodeling markers. Treatment with ruthenium red, a MCU inhibitor, restored systolic and diastolic dimensions, and partially restored EF, in part due to $\Delta\Psi m$ recovery in heart mitochondria.[38] In another study, Zaglia et al[13] associated the upregulation of MCU and cardiac hypertrophy in pressure overload induced by transaortic banding.[13] Moreover, by locking pressure overload, induced hypertrophy and remodeling prevented MCU overexpression as a corroboration of the pressure-induced tissue adaptation. These data are in accordance with our study where we found a direct correlation between MCU expression with mouse heart hypertrophy and with diastolic and systolic dimensions in failing human hearts, preventing cell hypertrophy by silencing or inhibiting MCU in rat cardiomyocytes and rat myoblast cells under prohypertrophic ANGII treatment.

The mechanisms regulating MCU upregulation remain to be fully understood in HF. There is growing evidence of a potential mechanism mediating MCU expression by activating CREB.[32,48,49] CREB plays a critical role in gene expression regulation in response to various extracellular signals, such as Ca^{2+}-dependent mitochondrial metabolism in B lymphocytes.[32] In HF, the role of CREB is controversial. It has been discussed as a negative apoptosis regulator in dilated cardiomyopathy and ischemia-reperfusion injury.[50] However, there are reports of CREB Ser133 phosphorylation and activation of the CRE-mediated gene transcription under chronic β-adrenergic stimulation.[33,51] The phosphorylation of Ser133 residue induces the transcriptional activity of CREB, which seems involved in heart remodeling.[52] In another study, Shanmughapriya et al[48] showed a Ca^{2+}-dependent and cyclic adenosine monophosphate signaling activation of CREB with direct upregulation in MCU expression by phosphorylated CREB in B lymphocytes.

In addition to CREB, CAMKII has been associated as an MCU expression promoter in a Ca^{2+}-dependent manner.[53] Moreover, knocking down CAMKII significantly mitigated CREB phosphorylation, MCU upregulation, and MCU-mediated mitochondrial oxidative stress.[54] Our study replicated these previous findings,

FIGURE 8 Scheme of the Proposed Mechanisms for ANGII-Induced MCU Overexpression Through Ca^{2+}-Dependent CAMKII/CREB Activation Signaling and mCa^{2+} Overload-Dependent Cardiomyocytes Hypertrophy Through ROS-Mediated NF-κB Activation

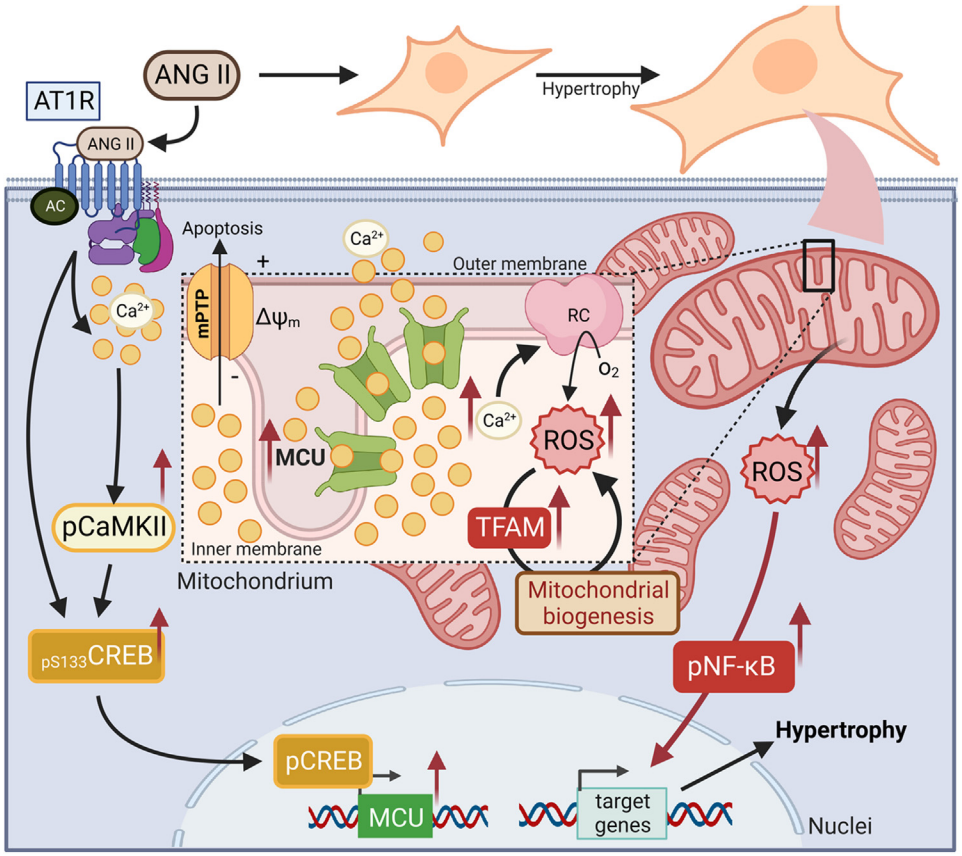

ΔΨm = mitochondrial membrane potential; AT1R = angiotensin II receptor type 1; mPTP = mitochondrial permeability transition pore; other abbreviations as in Figures 1 to 3.

describing for the first time in HF a mechanism of Ca^{2+}-dependent upregulation of MCU by ANGII induced by transcriptional activation of CREB and CaMKII in a time-dependent manner. Here, the signaling pathway of CREB activation by ANGII is characterized by CAMKII phosphorylation (peak at 3 hours), followed by CREB phosphorylation (peak at 12 hours), then increasing MCU protein expression (peak at 24 hours). Although the phosphorylation of CAMKII was studied primarily as an activation induced by Ca^{2+} and is described as intermediary signaling in the MCU transcriptional regulation.[53,55]

Considering all these results, we propose a mechanism for mCa^{2+} overload-induced cardiac remodeling through MCU upregulation through a Ca^{2+}-dependent CAMKII/CREB activation signaling, leading to mROS-mediated NF-κB activity (Figures 5 and 8).

There are 2 major points that are currently under analysis and still missing a consensual theory. One is the impact of the modified expression of MCU complex proteins and their stoichiometry in HF.[35,36,56] One of those proteins is MICU1, which works as an MCU gate and define sensibility and Ca^{2+}-dependent activation threshold of the MCU pore to Ca^{2+} through a fine stoichiometric balance between both proteins that can induce a more sensible MCU, and thus, an increment in mCa^{2+} overload.[56] Here, in nonischemic human HF, we describe a mouse model of HF and a cellular model of ANGII-induced remodeling and upregulation of MCU which is consistent with a metabolic adaptation of the tissue and cells to an increased pressure workload and an intracellular Ca^{2+} signaling that is triggered to match ATP production to the energy demand. Additional analysis of MCU regulatory proteins and their protein stoichiometry will

further contribute for the understanding of HF.[56] The second point under analysis involves determining the role of sarcoplasmic reticulum-mitochondria cross-talk through MCU (in mCa^{2+} overload and metabolic adaptation in HF), which is not fully understood nor addressed in this work. However, it justifies further investigation, as it may constitute a key mechanism responsible for the onset and maintenance of excitation-contraction coupling and a proposed regulator effect of MCU, which by proximity has been shown to be determinant in mCa^{2+} handling.[57] Moreover, when augmented Ca^{2+} release is promoted acutely, it leads to a mCa^{2+} overload followed by the generation of mROS and to a consequently increased sensibility to activation of the mPTP.[58]

Numerous findings have shown mitochondrial dysfunction and Ca^{2+} mishandling to be key players in mediating cardiac dysfunction and cardiac hypertrophy in HF.[21,59] Consistently, we have shown that the mCa^{2+} overload is the driver signal underlying a chronic pathologic mechanism of remodeling in HF depending on oxidative stress generated by mROS. Thus, following mCa^{2+} overload induction, not only by the upregulation of MCU in shMock cells exposed to ANGII, but also by inhibiting the NCLX in MCU-silenced cells, we observed an increase in the generation of mROS followed by cell hypertrophy. This was prevented either by blocking mROS with a specific mitochondrial anion superoxide scavenger, Mito-TEMPO, or inhibiting MCU, and thus mCa^{2+} influx leading to overload, with Ru_{360} in shMock cells exposed to ANGII. This corroborates the importance of mCa^{2+}-induced reactive oxygen species (ROS) in the underlying remodeling mechanism, as indicated by others.[60]

Growing evidence has shown ROS-mediated NF-κB signaling. For example, Takada et al[61] have shown that ROS influences the activation of the NF-κB pathway primarily by inhibiting the phosphorylation of the nuclear factor of the kappa light polypeptide gene enhancer in the B-cell inhibitor alpha. In chronic conditions, NF-κB activation is reported to be detrimental, promoting HF by eliciting chronic proinflammatory and cardiac hypertrophy programs.[62,63] Similarly, in our study, mCa^{2+}-dependent ROS generation by ANGII led to increased activation of NF-κB. However, silencing MCU avoided mCa^{2+} overload and ROS generation, preventing NF-κB activation. Therefore, we did not observe the upregulation of remodeling and proinflammatory markers. In this respect, our results are in accordance with previous studies showing that pathologic remodeling can be prevented by blocking ROS-dependent NF-κB transcriptional activation.[64]

Mitochondrial biogenesis may also play a role in the generation of ROS and may further potentiate NF-κB phosphorylation. Liu et al[27] have shown that mCa^{2+} overload, through MCU upregulation, inhibits the phosphorylation of TFAM, and thus enhances its stability to promote mitochondrial biogenesis, followed by an increase in ROS production and the subsequent activation of NF-κB signaling. In agreement with our results, it is possible that mitochondrial biogenesis may play a role in HF remodeling by participating in the activation of proinflammatory and remodeling programs dependent on NF-κB phosphorylation.

Diseases such as HF are a growing socioeconomic burden; therefore, developing new therapies based on novel therapeutic targets that can revolutionize disease management is important. Disruption of mCa^{2+} handling is intimately related to the pathophysiology of HF and targeting Ca^{2+}-handling proteins have been proposed.[12] Our data consistently unravel a potential target for preventing cardiac remodeling and mitochondrial dysfunction by targeting MCU, whether by genetic deletion or pharmacologic inhibition using Ru_{360}. In this context, the field of nanomedicine has attracted much attention as several studies have shown that using nanoparticles could increase drug use efficiency to improve cardioprotection or treatment in HF.[65,66] In HF, it has been shown that damaged cardiac tissue offers better nanoparticle internalization efficiency than healthy tissue[15], opening the panoply of therapies and new hypotheses, including the development of studies around the pharmacologic inhibition of MCU.[12]

STUDY LIMITATIONS. Although our data consistently show the importance of mCa^{2+} handling in cardiac remodeling, there are some limitations to the study to be considered: (1) In our study with human LV tissue samples, the scarce availability of tissue limited further studies to corroborate and explore the underlying mechanism found in our cellular model. (2) The studies performed to assess mitochondrial density are not deeply developed, and further experiments using the proper tools are required to fully understand the impact of mitochondrial calcium and ROS alterations in HF impact on mitochondrial network, biogenesis, and potential mitophagy. (3) Our cellular model of cardiac myoblast may not be entirely representative of human cardiac tissue, and the translation of our findings is sustained on hypothesizing upon the correlations between

MCU upregulation, hypertrophy, and mitochondrial dysfunction. Therefore, to translate the findings, we assessed the role of MCU in hypertrophy in other models: in the LV of hypertrophic hearts from an ANGII-induced mouse model of HF and MCU loss-of-function in neonatal rat cardiomyocyte primary culture. These data, together with other reports using animal models or primary culture of cardiomyocytes, corroborate the proposed underlying mechanisms.

CONCLUSIONS

In HF, mCa^{2+} overload mediates cardiomyocyte hypertrophy and mitochondrial dysfunction through a proposed complex adaptive mechanism involving Ca^{2+}-dependent MCU upregulation through CREB/CAMKII signaling and Ca^{2+}-mediated mROS generation and activation of NF-κB-mediated hypertrophic and proinflammatory program. This reveals a novel mechanism underlying mCa^{2+}-mediated pathologic remodeling and provides a potential pharmacological target for HF.

ACKNOWLEDGMENTS This work was a research program from the Cardiovascular Medicine Research Group - Tecnológico de Monterrey, and Experimental Medicine and Advanced therapies - The Institute for Obesity Research, Tecnológico de Monterrey. The authors thank Noemi García and Julio Altamirano for their support and valuable discussions, Carlos Campero for his support in the cell transfection protocol, and Nestor Rubio for the support with the animal model of heart failure with reduced ejection fraction.

FUNDING SUPPORT AND AUTHOR DISCLOSURES

This work was partially supported by the CONACYT Grants 256577, 258197, Fronteras de la Ciencia Grant (0682). The authors have reported that they have no relationships relevant to the contents of this paper to disclose.

ADDRESS FOR CORRESPONDENCE: Dr Gerardo García Rivas, Hospital Zambrano Hellion 2° piso, Av. Batallón de San Patricio 112, Real San Agustín, 66278, San Pedro Garza García, NL, Mexico. E-mail: gdejesus@tec.mx.

PERSPECTIVES

COMPETENCY IN MEDICAL KNOWLEDGE: This study contributes to the knowledge of the pathophysiology of chronic pressure overload-induced HF with supporting clinical and preclinical data. We describe and propose a novel role for mCa^{2+} overload in cardiac remodeling associated with changes in the expression of the MCU as the result of a metabolic adaptation of the tissue. Our studies further suggest that therapeutic targeting of MCU in HF has a potential application and may lead to the prevention or improvement of cardiac remodeling but will still require additional preclinical studies to ensure the safety of this approach.

TRANSLATIONAL OUTLOOK: The underlying mechanisms responsible for cardiac remodeling and energetic dysfunction in chronic pressure overload-induced HF are still controversial. We show the role of mCa^{2+} overload in mROS-mediated cardiac myoblast remodeling induced by ANGII and how this signaling is mediated by the upregulation of MCU through a Ca^{2+}-dependent CREB/CAMKII transcriptional activation. Furthermore, by targeting MCU (gene silencing or pharmacological inhibition), we could prevent cell remodeling and mitochondrial dysfunction. We have shown a correlation between MCU expression in human LV from nonischemic HF with reduced EF, cardiac function (negative correlation), and remodeling (positive correlation). Remarkably, after LVAD implantation, in which cardiac pressure overload is reduced, MCU expression decreases. These latter translationally oriented studies suggest a potential metabolic adaptive mechanism in which mCa^{2+} handling through MCU may participate in the signaling events driving cardiac remodeling and energetic dysfunction, and that further preclinical studies will be required before this mechanism and potential therapy can be proven and advanced safely into clinical trials of patients with HF.

REFERENCES

1. Bers DM. Cardiac excitation–contraction coupling. *Nature*. 2002;415(6868):198–205.

2. Glancy B, Balaban RS. Role of mitochondrial Ca2+ in the regulation of cellular energetics. *Biochemistry*. 2012;51(14):2959–2973.

3. Kwong JQ, Lu X, Correll RN, et al. The mitochondrial calcium uniporter selectively matches metabolic output to acute contractile stress in the heart. *Cell Rep*. 2015;12(1):15–22.

4. Zhou B, Tian R. Mitochondrial dysfunction in pathophysiology of heart failure. *J Clin Invest*. 2018;128(9):3716–3726.

5. Xu HX, Cui SM, Zhang YM, Ren J. Mitochondrial Ca2+ regulation in the etiology of heart failure: physiological and pathophysiological implications. *Acta Pharmacol Sin*. 2020;41(10):1301–1309.

6. Feno S, Rizzuto R, Raffaello A, Vecellio Reane D. The molecular complexity of the mitochondrial calcium uniporter. *Cell Calcium*. 2021;93:102322.

7. D'Angelo D, Rizzuto R. The mitochondrial calcium uniporter (MCU): molecular identity and role in human diseases. *Biomolecules*. 2023;13(9):1304.

8. Luongo TS, Lambert JP, Yuan A, et al. The mitochondrial calcium uniporter matches energetic supply with cardiac workload during stress

and modulates permeability transition. *Cell Rep*. 2015;12(1):23–34.

9. De La Fuente S, Lambert JP, Nichtova Z, et al. Spatial separation of mitochondrial calcium uptake and extrusion for energy-efficient mitochondrial calcium signaling in the heart. *Cell Rep*. 2018;24(12):3099–3107.

10. De J García-Rivas G, Carvajal K, Correa F, Zazueta C. Ru360, a specific mitochondrial calcium uptake inhibitor, improves cardiac post-ischaemic functional recovery in rats in vivo. *Br J Pharmacol*. 2006;149(7):829–837.

11. Fernández-Sada E, Silva-Platas C, Villegas CA, et al. Cardiac responses to β-adrenoceptor stimulation is partly dependent on mitochondrial calcium uniporter activity. *Br J Pharmacol*. 2014;171(18):4207–4221.

12. Lozano O, Marcos P, Salazar-Ramirez FdJ, Lázaro-Alfaro AF, Sobrevia L, García-Rivas G. Targeting the mitochondrial Ca2+ uniporter complex in cardiovascular disease. *Acta Physiologica (Oxf)*. 2023;237(4):e13946.

13. Zaglia T, Ceriotti P, Campo A, et al. Content of mitochondrial calcium uniporter (MCU) in cardiomyocytes is regulated by microRNA-1 in physiologic and pathologic hypertrophy. *Proc Natl Acad Sci U S A*. 2017;114(43):E9006–E9015.

14. Rickham PP. Human experimentation. Code of ethics of the World Medical Association. Declaration of Helsinki. *Br Med J*. 1964;2(5402):177.

15. Ruiz-Esparza GU, Segura-Ibarra V, Cordero-Reyes AM, et al. A specifically designed nanoconstruct associates, internalizes, traffics in cardiovascular cells, and accumulates in failing myocardium: a new strategy for heart failure diagnostics and therapeutics. *Eur J Heart Fail*. 2016;18(2):169–178.

16. Pacher P, Nagayama T, Mukhopadhyay P, Bátkai S, Kass DA. Measurement of cardiac function using pressure–volume conductance catheter technique in mice and rats. *Nat Protoc*. 2008;3(9):1422–1434.

17. Vicencio JM, Ibarra C, Estrada M, et al. Testosterone induces an intracellular calcium increase by a nongenomic mechanism in cultured rat cardiac myocytes. *Endocrinology*. 2006;147(3):1386–1395.

18. Oropeza-Almazán Y, Vázquez-Garza E, Chapoy-Villanueva H, Torre-Amione G, García-Rivas G. Small interfering RNA targeting mitochondrial calcium uniporter improves cardiomyocyte cell viability in hypoxia/reoxygenation injury by reducing calcium overload. *Oxid Med Cell Longev*. 2017;2017:5750897.

19. Basualto-Alarcón C, Jorquera G, Altamirano F, Jaimovich E, Estrada M. Testosterone signals through mTOR and androgen receptor to induce muscle hypertrophy. *Med Sci Sports Exerc*. 2013;45(9):1712–1720.

20. Altamirano F, Oyarce C, Silva P, et al. Testosterone induces cardiomyocyte hypertrophy through mammalian target of rapamycin complex 1 pathway. *J Endocrinol*. 2009;202(2):299–307.

21. Smith JG. Molecular epidemiology of heart failure: translational challenges and opportunities. *J Am Coll Cardiol Basic Trans Science*. 2017;2(6):757–769.

22. Garbincius JF, Luongo TS, Elrod JW. The debate continues — what is the role of MCU and mitochondrial calcium uptake in the heart? *J Mol Cell Cardiol*. 2020;143:163–174.

23. Doughan AK, Harrison DG, Dikalov SI. Molecular mechanisms of angiotensin II–mediated mitochondrial dysfunction. *Circ Res*. 2008;102(4):488–496.

24. Ruwhof C, Van Der Laarse A. Mechanical stress-induced cardiac hypertrophy: mechanisms and signal transduction pathways. *Cardiovasc Res*. 2000;47(1):23–37.

25. Dai DF, Johnson SC, Villarin JJ, et al. Mitochondrial oxidative stress mediates angiotensin II–induced cardiac hypertrophy and Gαq overexpression–induced heart failure. *Circ Res*. 2011;108(7):837–846.

26. Nisoli E, Tonello C, Cardile A, et al. Calorie restriction promotes mitochondrial biogenesis by inducing the expression of eNOS. *Science*. 2005;310(5746):314–317.

27. Liu Y, Jin M, Wang Y, et al. MCU-induced mitochondrial calcium uptake promotes mitochondrial biogenesis and colorectal cancer growth. *Signal Transduct Target Ther*. 2020;5(1):59.

28. Li Y, Ha T, Gao X, et al. NF-κ activation is required for the development of cardiac hypertrophy in vivo. *Am J Physiol Heart Circ Physiol*. 2004;287(4):H1712–H1720.

29. Luongo TS, Lambert JP, Gross P, et al. The mitochondrial Na +/Ca 2+ exchanger is essential for Ca 2+ homeostasis and viability. *Nature*. 2017;545(7652):93–97.

30. Mishra J, Jhun BS, Hurst S, O-Uchi J, Csordás G, Sheu SS. The mitochondrial Ca2+ uniporter: structure, function and pharmacology. *Handb Exp Pharmacol*. 2017;240:129–156.

31. de Jesús García-Rivas G, Guerrero-Hernández A, Guerrero-Serna G, Rodríguez-Zavala JS, Zazueta C. Inhibition of the mitochondrial calcium uniporter by the oxo-bridged dinuclear ruthenium amine complex (Ru360) prevents from irreversible injury in postischemic rat heart. *FEBS J*. 2005;272(13):3477–3488.

32. Shanmughapriya S, Rajan S, Hoffman NE, et al. Ca2+ signals regulate mitochondrial metabolism by stimulating CREB-mediated expression of the mitochondrial Ca2+ uniporter gene MCU. *Sci Signal*. 2015;8(366):ra23.

33. Liu Z, Zhao W, Yuan P, et al. The mechanism of CaMK2α-MCU-mitochondrial oxidative stress in bupivacaine-induced neurotoxicity. *Free Radic Biol Med*. 2020;152:363–374.

34. Bhat PK, Ashwath ML, Rosenbaum DS, Costantini O. Usefulness of left ventricular end-systolic dimension by echocardiography to predict reverse remodeling in patients with newly diagnosed severe left ventricular systolic dysfunction. *Am J Cardiol*. 2012;110(1):83–87.

35. O'Rourke B, Ashok D, Liu T. Mitochondrial Ca2+ in heart failure: not enough or too much? *J Mol Cell Cardiol*. 2021;151:126–134.

36. Garbincius JF, Elrod JW. Is the failing heart starved of mitochondrial calcium? *Circ Res*. 2021;128:1205–1207.

37. Burkhoff D, Topkara VK, Sayer G, Uriel N. Reverse remodeling with left ventricular assist devices. *Circ Res*. 2021;128(10):1594–1612.

38. Yu Z, Chen R, Li M, et al. Mitochondrial calcium uniporter inhibition provides cardioprotection in pressure overload-induced heart failure through autophagy enhancement. *Int J Cardiol*. 2018;271:161–168.

39. Santulli G, Xie W, Reiken SR, Marks AR. Mitochondrial calcium overload is a key determinant in heart failure. *Proc Natl Acad Sci U S A*. 2015;112(36):11389–11394.

40. Liu T, Yang N, Sidor A, O'Rourke B. MCU overexpression rescues inotropy and reverses heart failure by reducing SR Ca2+ leak. *Circ Res*. 2021;128(8):1191–1204.

41. Wang P, Xu S, Xu J, et al. Elevated MCU expression by CaMKIIδB limits pathological cardiac remodeling. *Circulation*. 2022;145(14):1067–1083.

42. Rasmussen TP, Wu Y, Joiner MLA, et al. Inhibition of MCU forces extramitochondrial adaptations governing physiological and pathological stress responses in heart. *Proc Natl Acad Sci U S A*. 2015;112(29):9129–9134.

43. Harkins S, Whitton JL. Chromosomal mapping of the αMHC-MerCreMer transgene in mice reveals a large genomic deletion. *Transgenic Res*. [Internet]. *Transgenic Res*. 2016;25(5):639–648.

44. Lexow J, Poggioli T, Sarathchandra P, Santini MP, Rosenthal N. Cardiac fibrosis in mice expressing an inducible myocardial-specific Cre driver. *Dis Model Mech*. 2013;6(6):1470–1476.

45. Wiersma M, Van Marion DMS, Wüst RCI, et al. Mitochondrial dysfunction underlies cardiomyocyte remodeling in experimental and clinical atrial fibrillation. *Cells*. 2019;8(10):1202.

46. Michels G, Khan IF, Endres-Becker J, et al. Regulation of the human cardiac mitochondrial Ca2+ uptake by 2 different voltage-gated Ca2+ channels. *Circulation*. 2009;119(18):2435–2443.

47. Paillard M, Huang KT, Weaver D, Lambert JP, Elrod JW, Hajnóczky G. Altered composition of the mitochondrial Ca2+ uniporter in the failing human heart. *Cell Calcium*. 2022;105:102618.

48. Faccenda D, Gorini G, Jones A, et al. The ATPase Inhibitory Factor 1 (IF1) regulates the expression of the mitochondrial Ca2+ uniporter (MCU) via the AMPK/CREB pathway. *Biochim Biophys Acta Mol Cell Res*. 2021;1868(1):118860.

49. Haack KKV, Mitra AK, Zucker IH. NF-κB and CREB are required for angiotensin II type 1 receptor upregulation in neurons. *PLoS One*. 2013;8(11):e78695.

50. Fentzke RC, Korcarz CE, Lang RM, Lin H, Leiden JM. Dilated cardiomyopathy in transgenic mice expressing a dominant-negative CREB transcription factor in the heart. *J Clin Invest*. 1998;101(11):2415–2426.

51. Müller FU, Bokník P, Knapp J, et al. Activation and inactivation of cAMP-response element-mediated gene transcription in cardiac myocytes. *Cardiovasc Res*. 2001;52(1):95–102.

52. Ichiki T. Role of cAMP response element binding protein in cardiovascular remodeling: good, bad, or both? *Arterioscler Thromb Vasc Biol*. 2006;26(3):449–455.

53. Nguyen EK, Koval OM, Noble P, et al. CaMKII (Ca2+/calmodulin-dependent kinase II) in mitochondria of smooth muscle cells controls mitochondrial mobility, migration, and neointima formation. *Arterioscler Thromb Vasc Biol*. 2018;38(6):1333–1345.

54. Wong MH, Samal AB, Lee M, et al. The KN-93 molecule inhibits calcium/calmodulin-dependent protein kinase II (CaMKII) activity by binding to Ca2þ/CaM. *J Mol Biol*. 2019;431(7):1440–1459.

55. Luczak ED, Anderson ME. CaMKII oxidative activation and the pathogenesis of cardiac disease. *J Mol Cell Cardiol*. 2014;73:112–116.

56. Chapoy-Villanueva H, Silva-Platas C, Gutiérrez-Rodríguez AK, et al. Changes in the stoichiometry of uniplex decrease mitochondrial calcium overload and contribute to tolerance of cardiac ischemia/reperfusion injury in hypothyroidism. *Thyroid*. 2019;29(12):1755–1764.

57. Salazar-Ramírez F, Ramos-Mondragón R, García-Rivas G. Mitochondrial and sarcoplasmic reticulum interconnection in cardiac arrhythmia. *Front Cell Dev Biol*. 2021;8:623381.

58. Eisner V, Csordás G, Hajnóczky G. Interactions between sarco-endoplasmic reticulum and mitochondria in cardiac and skeletal muscle — pivotal roles in Ca^{2+} and reactive oxygen species signaling. *J Cell Sci*. 2013;126(Pt 14):2965–2978.

59. Nakamura M, Sadoshima J. Mechanisms of physiological and pathological cardiac hypertrophy. *Nat Rev Cardiol*. 2018;15(7):387–407.

60. Garbincius JF, Luongo TS, Jadiya P, et al. Enhanced NCLX-dependent mitochondrial Ca 2+ efflux attenuates pathological remodeling in heart failure. *J Mol Cell Cardiol*. 2022;167:52–66.

61. Takada Y, Mukhopadhyay A, Kundu GC, Mahabeleshwar GH, Singh S, Aggarwal BB. Hydrogen peroxide activates NF-kappa B through tyrosine phosphorylation of I kappa B alpha and serine phosphorylation of p65: evidence for the involvement of I kappa B alpha kinase and Syk protein-tyrosine kinase. *J Biol Chem*. 2003;278(26):24233–24241.

62. Li Y, Ha T, Gao X, et al. NF-kappaB activation is required for the development of cardiac hypertrophy in vivo. *Am J Physiol Heart Circ Physiol*. 2004;287(4).

63. Gopi V, Subramanian V, Manivasagam S, Vellaichamy E. Angiotensin II down-regulates natriuretic peptide receptor-A expression and guanylyl cyclase activity in H9c2 (2-1) cardiac myoblast cells: role of ROS and NF-κB. *Mol Cell Biochem*. 2015;409(1-2):67–79.

64. Gupta S, Young D, Maitra RK, et al. Prevention of cardiac hypertrophy and heart failure by silencing of NF-κB. *J Mol Biol*. 2008;375(3):637–649.

65. Lozano O, Lázaro-Alfaro A, Silva-Platas C, et al. Nanoencapsulated quercetin improves cardioprotection during hypoxia-reoxygenation injury through preservation of mitochondrial function. *Oxid Med Cell Longev*. 2019;2019:7683051.

66. Salazar-Ramírez FdJ, Lozano O, Chapoy-Villanueva H, Torre-Amione G, García-Rivas G. Developing a new polymeric system for release of immunomodulators for treatment of heart failure. *FASEB J*. 2018;32(S1):675.13-675.13.

KEY WORDS heart failure, mitochondrial calcium overload, mitochondrial calcium uniporter, mitochondrial dysfunction, pathological remodeling, reactive oxygen species

APPENDIX For supplemental tables and figures, please see the online version of this paper.